Last Glacial Maximum Climate and Atmospheric Circulation over the Australian Region from Climate Models

Yanxuan Du[1], Josephine R. Brown[1], J. M. Kale Sniderman[1]

[1] School of Geography, Earth and Atmospheric Sciences, University of Melbourne, Parkville, VIC, Australia

Correspondence to: Yanxuan Du (yanxuand@student.unimelb.edu.au)

Abstract. The Last Glacial Maximum (LGM, ~21,000 years ago) was the most recent time that the Earth experienced global maximum ice volume and minimum eustatic sea level. The climate changes over the Australian region at the LGM remain uncertain. In this study, five Coupled Model Intercomparison Project Phase 6 (CMIP6) models and eight Coupled Model Intercomparison Project Phase 5 (CMIP5) models that were included in the Paleoclimate Modelling Intercomparison Project (PMIP) Phases 3 and 4 are used to investigate regional climate (temperature, precipitation, and wind) over Australia at the LGM. The model simulations are compared with existing proxy records and other modelling studies. All models simulate consistent annual and seasonal cooling over the Australian region (defined as 0-45°S, 110°E-160°E) with a multi-model mean 2.9°C decrease in annual average surface air temperature over land at the LGM compared to pre-industrial. While models show consistent patterns of regional cooling over Australia at the LGM, the changes in precipitation differ between models. The simulated precipitation changes over tropical Australasia appear to be driven by changes in circulation and moisture transport, which vary greatly between models. Surface moisture balance calculated from precipitation minus evaporation shows little change over much of the Australian land area at the LGM. Changes in the strength and position of the mid-latitude westerlies are also uncertain, with wide model disagreement. These results indicate that climate models do not have a robust response in either tropical or mid-latitude circulation to LGM boundary conditions, suggesting that caution is required when using output from a single model in this region. Further analysis is required to determine the drivers of model circulation changes in this region and to identify the most plausible set of LGM simulations before quantitative model-proxy comparison can be attempted.

1 Introduction

The Last Glacial Maximum (LGM, ~21,000 years ago) refers to the coldest interval within the last glacial period, featuring global maximum ice volume and associated low eustatic sea-level (Clark et al., 2009). Ice sheets covered large parts of North America, Europe, and Northern Eurasia at this time (Ehlers and Gibbard, 2007). In Australia, Reeves et al. (2013a) present evidence of small glaciers in the Snowy Mountains of southeast Australia and Tasmania, with the most significant glacier advance at around 19.1 ka (Petherick et al., 2013). Global mean surface air temperature (SAT) estimates during the LGM range from 3.4 to 8.3 °C cooler than pre-industrial based on different model ensemble results constrained with proxy data (Schneider von Deimling et al., 2006; Holden et al., 2010; Annan and Hargreaves, 2013; Tierney et al., 2020a; Seltzer et al.,

Deleted: U

Deleted: U

Deleted: The Last Glacial Maximum (LGM, ~21,000 years ago) was the most recent time that the Earth experienced global maximum ice volume and minimum eustatic sea level, however,. tThe regional climate changes over the Australian region at the LGM remain uncertainunclear. In this study, fFiveour Coupled Model Intercomparison Project Phase 6 (CMIP6) models and eight Coupled Model Intercomparison Project Phase 5 (CMIP5) models that were included in the Paleoclimate Modelling Intercomparison Project (PMIP) Phases 3 and 4 were used in this research to investigate the regional temperature, precipitation, and windclimate (temperature, precipitation, and wind) changes and associated atmospheric circulation changes over Australia at the LGM relative to pre-industrial (PI), and compare the cresults onsistency with existing proxy records and other modelling studies. The annual multi-model mean (MMM) Australian land surface temperature is estimated to cool by 2.6 °C at the LGM. AlAll ofl our model resultss show consistent annual cooling over the Australian region (0-45°S, 110°E-160°E) with a multi-model mean (MMM) of 2.94°C decrease in land surface air temperature at the LGM compared to PI. The LGM – PI regional precipitation patterns over Australia show larger model disagreements compared to temperature changes. MMM annual precipitation decreased by 0.16 mm/day at the LGM relative to PI over modern Australian mainland areas (10°S-45°S, 110°E-160°E). Simulations of LGM pPrecipitation minus evaporation patterns changes relative to PI over Australia are also examined to assess the changes in Australian moisture balance at the LGM, however, model results . Despite reduced LGM precipitation, the greater decrease in LGM evaporation leads to a slightly positive moisture balance in many regions. This is in disagreement disagreed with some most proxy-based hydroclimatee reconstructions of reduced LGM moisture over Australia., This may partly reflect the fact that is increasingly recognised as a problem due to the lack of considerations for atmospheric CO_2 effects during the interpretations of most vegetation-based proxy records, that leads to large uncertainties in Australian LGM proxy-based hydroclimate reconstructions. Similar to previous studies, which might be due to the interpretations of vegetation-based proxy records or the uncertainties in model representation of moisture fluxes. lWe find a small equatorward multi-model average displacement of the boundary line between Southern Hemisphere (SH) westerly and easterly winds at the LGM but large model disagreements on the a shift in SH mid-latitude westerly winds at the LGMsimulations of LGM wind patterns are also observed, similar to previous studies, which may be mainly due to the uncertainties in different model configurations. This research provides a preliminary analysis and evaluation of the regional climate changes over the Australian region at the LGM. Nevertheless, ... [1]

Deleted: ca. 28-18 thousand years ago (ka)

Deleted: .

Deleted: It was a time of

Deleted: &

Deleted: glaciation

Deleted: S

Deleted: ¶
→

Deleted: &

2021; Annan et al., 2022) with recent studies suggesting a narrower range of 4.5 °C ± 0.9 °C (Annan et al., 2022) or 5.7 °C to 6.5 °C (Tierney et al., 2020a) depending on the method used. The global sea level was estimated at ca.120 meters lower than today (Lambeck et al., 2014; Yokoyama et al., 2018), resulting in the expansion of the land areas in many parts of the world, appearance of land bridges and the exposure of Sunda and Sahul shelves in Southeast Asia, which further allowed human migration during this period (Clarkson et al., 2017). The Australian mainland expanded at the LGM, connected by land bridges to New Guinea, Tasmania, and many smaller islands into a single landmass known as "Sahul" (Clarkson et al., 2017, see Figure 1 with the grey shading covering the land areas).

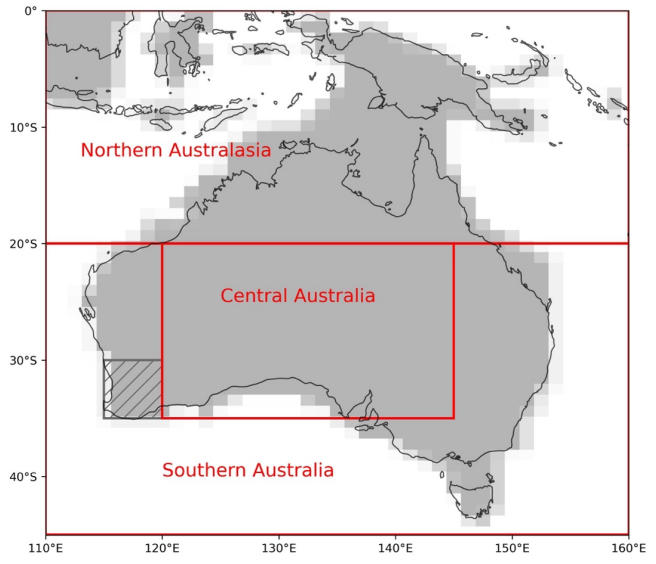

Figure 1: Classification of Northern Australasia, Central, and Southern Australia domains shown by red rectangles with modern day coastlines. The Central Australia domain is a subset of the larger Southern Australia domain. The south-west box for detecting JJA frontal precipitation that is most sensitive to westerlies is also indicated in hashes in the Southern Australia domain. The background grey shading indicates LGM land mask from CCSM4 model, plotted over modern coastlines.

LGM vegetation was also very different from today. There was a large reduction in area covered by boreal and temperate forests in northern mid- to high latitudes, expanded lowland tundra in Eurasia, expansion of savanna and grasslands at the margin of Amazon tropical forests and replacement of some areas of tropical forest in Africa, China and

Deleted: values of

Deleted: and

Deleted: b

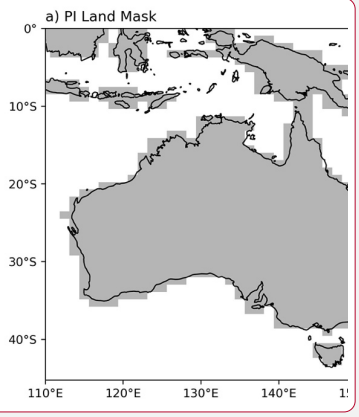

Deleted:

Deleted: ¶
Figure 1: Example of modern day (a) and LGM (b) land masks (shown as grey shading) from CCSM4 model, plotted over modern coastline¶

Southeast Asia with savanna, woodland and grassland (Prentice et al., 2011). These changes are associated with large LGM reduction in terrestrial biomass, caused by a combination of lower temperatures, changes in hydroclimate (moisture availability), and/or lower atmospheric CO_2 concentrations (~180 ppm) that cooled the climate and restricted vegetation growth (Scheff et al., 2017; Prentice et al., 2022). Dust suspension and transport was estimated to be more active at the LGM, which was possibly driven by stronger winds and drier climate conditions, particularly in the tropical and high-latitude regions (Lamy et al., 2014), or may have been partly a consequence of the reduced ability of terrestrial vegetation to stabilize soils (Scheff et al., 2017; Roderick et al., 2015).

The LGM is commonly recognised as a time of global cooling and lower sea levels, best estimates placing this at ca. 21 ka (Hughes et al., 2013). However, changes in Southern Hemisphere (SH) regional temperature, rainfall and atmospheric circulation are less well understood. In the SH, on landmasses remote from continental ice sheets, it has become clear from pollen and other terrestrial climate proxies that full glacial conditions were maintained in New Zealand and Australia between ca. 28-18 ka (Newnham et al., 2007; Cadd et al., 2021), which Newnham et al. (2007) referred to as the 'extended LGM'. Understanding the changes in regional climate over Australia at the LGM is of interest for a number of reasons. The Australian climate is influenced by major tropical and extratropical modes of circulation, including the Walker circulation and SH Hadley Cell, Indo-Australian monsoon and mid-latitude westerlies. Therefore, understanding how the climate of Australia changed at the LGM could provide insight into the changes in these large-scale climate processes. In addition, it is also crucial for interpreting records of human occupation (Williams et al., 2013; Bird et al., 2016; Bradshaw et al., 2021) and changes in flora and fauna distributions (Byrne et al., 2008; Nevill et al., 2010; Pepper and Keogh, 2021) from this period.

A limited number of climate modelling studies have focused on conditions during the LGM in the SH (e.g. Rojas et al., 2009; Rojas, 2013; Sime et al., 2013), with even fewer studies examining simulations of LGM climate in Australia (e.g. Hope, 2005; Yan et al., 2018). Some studies (e.g. Brown et al., 2020; Kageyama et al., 2021; Wang et al., 2023) have begun to explore the new PMIP4 simulations of LGM climate, but there has been little research on the changes in SH climate, including the Australian region in these simulations (or the older PMIP3 ensemble). This study investigates the climate (temperature, precipitation, moisture balance and wind) changes during the LGM relative to PI over the Australian region using available simulations from PMIP3/PMIP4 models and compares the results with existing proxy records and other model studies of the region. The aim is to provide preliminary insights into the LGM climate in Australia from model simulations and evaluate the model consistency with available proxy records.

1.1 Palaeoenvironmental proxy records for the Australian LGM

This section summarises the available proxy records across the Australian region separated into three distinct climate zones (see Figure 1 and Section 2.3 for the classification and map) from the period 24 to 18 ka as broadly representative of LGM reconstructed climate in Australia. The regional comparisons with our model simulation results are presented in the Discussion (Section 4).

Deleted: Many regions that are forested today were covered in tundra and grasslands at the LGM (Kageyama et al., 2017)…
Deleted: reflect
Deleted: related to
Deleted: s
Deleted: ; Ujvari et al., 2018
Deleted: stabilise
Deleted: Southern Hemisphere
Deleted: understanding LGM climate in Australia
Deleted: and relative atmospheric circulation
Deleted: ,
Deleted: in Australia
Deleted: of
Deleted: compared to PI
Deleted: , which also allows examining the reliability of proxy reconstructions in Australia..
.
Deleted: .
Deleted: The exact definition of the LGM has varied over time. Traditionally, the concept has denoted the time of maximum global ice volume and/or minimum eustatic sea level, best estimates placing this at ca. 21 ka (Hughes et al., 2013). However, in the Southern Hemisphere (SH), on landmasses remote from continental ice sheets, it has become clear from pollen and other terrestrial climate proxies that full glacial conditions were maintained in New Zealand and Australia between ca. 28-18 ka (Newnham et al., 2007; Cadd et al., 2021), which Newnham et al. (2007) referred to as the 'extended LGM'. In general, this study will discuss proxy climate records from the period from 28 to 18 ka as broadly representative of LGM climate and compare those records with our model results for temperature, precipitation, and wind patterns over Australia.¶
Deleted: The LGM is commonly recognised as a time of global cooling and lower sea levels, but changes in SH regional temperature, rainfall and atmospheric circulation are less well understood. A limited number of climate modelling studies have focused on conditions during the LGM in the SH (e.g. Rojas et al., 2009; Rojas, 2013), with even fewer studies examining simulations of LGM climate in Australia (e.g. Hope, 2005; Yan et al., 2018). Some studies (e.g. Kageyama et al., 2021; Annan & Hargreaves, 2013; DiNezio & Tierney, 2013; Sime et al., 2013) have begun to explore the new PMIP4 simulations of LGM climate, but there has been little research on the changes in SH climate, including the Australian region in these simulations (or the older PMIP3 ensemble). Therefore, this study aims to investigate the climate (temperature, precipitation, moisture balance and wind) changes at the LGM over the Australian region, making use of available PMIP3 and PMIP4 climate model simulations of LGM climate.¶
Deleted: the
Deleted: proxy-

In northern Australia (see Figure 1 for corresponding region), surrounding sea surface temperatures (SSTs) are estimated to have cooled by 1 to 3 °C at the LGM relative to present (Reeves et al., 2013a). The temperature in upland areas in New Guinea is estimated to have reduced by 4 to 6 °C compared to present based on pollen records from near treeline in the Kosipe Valley (Hope, 2009). A dramatic reduction in tree cover was identified at the LGM in tropical savanna woodland in northern Australia from pollen and geochemical records (Rowe et al., 2021). Rowe et al. (2021) attributed the change in vegetation to a combination of a cooler and drier glacial climate, while also considering the possible role of lower atmospheric CO_2 concentrations and the increased distance of the site from the coastline. Reduced fire activity occurred as a result of less available fuel, indicating that the vegetation at the LGM was less influenced by fire events than today (Rowe et al., 2021). There is uncertainty about the drivers of LGM climate changes in northern Australia; sparser vegetation has been interpreted previously as a sign of aridity, but it is also likely that low CO_2 played a role in reducing plant biomass (e.g. Scheff et al., 2017; Prentice et al., 2017; Prentice et al., 2022). Denniston et al. (2013) found evidence of an active but variable monsoon during the LGM based on speleothem records at Ball Gown Cave in tropical northern Australia, with more positive speleothem isotopic values at the LGM than the late Holocene indicating relatively dry glacial conditions.

In southern Australia during the LGM, a SAT reduction of 4-6 °C has been inferred from pollen records, and SST cooling varying from 3 to 9 °C has been inferred in nearby ocean regions (Petherick et al., 2013). Fossil pollen records indicating widespread reductions in tree cover have often been interpreted as implying drier conditions, i.e. reduced precipitation and/or increased evaporation (Petherick et al., 2013), but the potential role of low atmospheric CO_2 in reducing plant productivity has rarely been considered in the region (Prentice et al., 2017; Sniderman et al., 2019). Moreover, regionally wetter conditions (increased precipitation and/or reduced evaporation) were also present in some parts of the Southern Australian domains (Reeves et al., 2013b), perhaps consistent with a northward shift of the SH westerlies at the LGM (Kohfeld et al., 2013). Some evidence of higher lake (Lakes Mungo, Keilambete and George) and river levels in the Murray-Darling Basin (Hesse et al., 2018) has been interpreted in terms of greater seasonal runoff due to snowmelt (Petherick et al., 2013), or some combination of higher precipitation and lower evapotranspiration (Hesse et al., 2018). In subtropical eastern Australia, the persistence of moisture-demanding woodlands suggests that the effective precipitation (net moisture) levels did not drop dramatically during the LGM in this region (Cadd et al., 2018).

In central Australia, the average LGM air temperature in the arid zone was estimated to decrease by 9 °C below present (Miller et al., 1997) based on amino-acid racemisation of emu eggshell. Fitzsimmons et al. (2013) argued that the arid interior experienced extensive dune activity and dust transport, reduced but episodic fluvial activity at the LGM relative to PI. However, there is geomorphological evidence for higher lake levels at Lake Frome (Cohen et al., 2015). Evidence of wetter conditions in arid Australia during the LGM was found by Treble et al. (2017) from speleothem records at Mairs Cave, Flinders Ranges in the Southern Australian semi-arid zone. That study suggested that the Flinders Ranges were relatively wet during the LGM, possibly associated with a southward shift of the Intertropical Convergence Zone (ITCZ), allowing more tropical moisture to reach the cave. These proxy records providing evidence of relatively wet conditions at the

Deleted: tropical Australasia
Deleted: 2
Deleted: the snowlines
Deleted: Moreover,
Deleted: that there is isotopic
Deleted: for LGM moisture as high as today
Deleted: in
Deleted: .
Deleted: temperate
Deleted: possibly associated
Deleted: the arid interior zone in
Deleted: and

LGM support the hypothesis proposed by De Deckker et al. (2020), that water was available during the cold and dry LGM period in Australia, sustaining human populations in inland areas.

In summary, there is evidence for widespread cooling over northern, southern and central Australia at the LGM based on a range of proxy records, with the largest cooling inland and at high elevations. In northern Australia, vegetation and fire records suggest drier conditions or possible influences from lower CO_2, while speleothem records may indicate drier conditions. Records from southern and central Australia provide uncertain evidence for hydroclimate change, with some records supporting wetter conditions and others implying drying. Moisture changes may reflect meridional shifts in the westerlies and tropical convergence zone, but evidence for these shifts is also contradictory.

1.2 Climate models simulations of the LGM

Many previous modelling studies have focused on the LGM as this period is one of the main "entry card" experiments for PMIP (Kageyama et al., 2017). However few studies have examined the Southern Hemisphere or the Australian region, as noted above. In this section, we summarise previous LGM modelling studies which focus on the Australian region and major modes of circulation including the Indo-Australian monsoon and the SH mid-latitude westerlies.

Several early studies made use of low-resolution climate models to examine the changes in the Australian monsoon over the late Quaternary (e.g. Wyrwoll and Valdes, 2003; Marshall and Lynch, 2006). In particular, Marshall and Lynch (2006) employed the FOAM model to simulate time-slices including the LGM and found that there was an overall drying over northern Australia at the LGM, with a slight increase during monsoon onset offset by drying during the monsoon peak and retreat. More recently, Yan et al. (2018) examined the Australian monsoon in PMIP3 simulations and found decreased annual and winter precipitation over northern Australia with increases in the early summer (November to December) due to enhanced moisture convergence. This study examines the changes in northern Australian temperature, precipitation and atmospheric circulation in a larger ensemble of models including five models from the latest CMIP6-PMIP4 generation.

The behaviour of the SH westerlies at the LGM is a major area of research with relevance for southern Australian climate. Previous modelling studies using coupled atmosphere-ocean models (PMIP2 and 3) and atmosphere-only models (PMIP1) show ambiguous results regarding the latitudinal positions of the SH mid-latitude westerlies during the LGM. For example, Sime et al. (2013) found strengthening and southward shifts in the maximum 850 hPa SH westerlies based on PMIP2 simulations with an atmosphere-only model (HadAM3). Similarly, a poleward shift in SH surface westerlies was indicated by Kitoh et al. (2001) from an AOGCM used in PMIP1 (MRI-CGCM1 model). However, disagreements are found between different models, with shifts equatorward (Kim et al., 2003) and no latitudinal change (Otto-Bliesner et al., 2006; Rojas et al., 2009) in SH westerlies also observed from PMIP model simulations. This disagreement across model simulations is consistent with a more recent study (Chavaillaz et al., 2013) using the more recent PMIP3 and CMIP5 models, suggesting no agreement was reached between models regarding the latitudinal changes in SH westerlies during the LGM. Rojas (2013) suggested that differences in response may be related to the coupling between atmosphere, ocean and sea ice in

Deleted: ¶

Deleted: for

Deleted:

Deleted: .

Deleted: T

Deleted: the Paleoclimate Modelling Intercomparison Project (

Deleted:)

Deleted: .

Deleted: and

Deleted: and

Deleted: and

Deleted: Some studies have used PMIP simulations with proxy data to reconstruct LGM climate (e.g. Annan & Hargreaves, 2013; DiNezio & Tierney, 2013; Sime et al., 2013). Other studies have compared results from a range of simulations including the LGM as well as historical or future climates (e.g. Chavaillaz et al., 2013; Brown et al., 2020; Liu et al., 2020), using past climates to provide insights into future climate change (Tierney et al., 2020b). This section summarises the relevant modelling studies for the SH LGM climate.¶

Deleted: In a recent study, Kageyama et al. (2021) presented global results from PMIP3 and PMIP4 LGM simulations and found that the multi-model global average change in temperature is similar for the two ensembles. The PMIP4 models simulate slightly drier annual precipitation changes in the LGM than the PMIP3 models. Overall, while there are large differences between individual models, the two groups of models are not fundamentally different. In addition, the LGM simulations were found to be broadly consistent with regional proxy reconstructions (Kageyama et al., 2021). In this study, the PMIP3 and PMIP4 LGM simulations are examined in more detail over Australia, considering seasonal anomalies and individual model responses as well as the ensemble mean.¶

Deleted: focused on understanding the climate system during the LGM, …

Deleted: variations gaps

Deleted: newer

the models. Shifts in SH westerlies and the influences on southern and central Australian climate in an ensemble of CMIP5-PMIP3 and CMIP6-PMIP4 models are investigated in this study.

Utilising LGM simulations from an ensemble of CMIP6-PMIP4 and CMIP5-PMIP3 models, this study provides a summary of changes in temperature, precipitation and winds over the Australian region, including both multi-model mean changes and evaluation of model spread or agreement. The drivers of precipitation changes are explored, with reference to changes in regional temperature and circulation patterns. Evidence for changes in the summer monsoon and the mid-latitude westerlies are also examined. The model simulations are compared with proxy reconstructions of temperature and precipitation or moisture balance to determine the extent of model-proxy agreement.

In this paper, the data and methods are described in Section 2, Section 3.1 presents temperature results from models, while wind and precipitation changes at the LGM relative to PI are shown in Section 3.2 and 3.3, respectively. Relationships between climate variables, such as SH mid-latitude westerly winds and precipitation changes at the LGM in JJA season, and the correlations between seasonal temperature and precipitation patterns are evaluated in Section 3.3.2 as drivers of precipitation change. Section 4 discusses the limitations and consistencies between relevant proxy records and modelling studies with our model results, followed by the conclusion in Section 4.4.

2 Data and methods

2.1 Model datasets

This study makes use of PMIP Phase 3 (PMIP3, Braconnot et al., 2012) model simulations which were included in the Coupled Model Intercomparison Project Phase 5 (CMIP5, Taylor et al., 2012), and PMIP Phase 4 (PMIP4, Kageyama et al., 2018) simulations which were included in CMIP Phase 6 (CMIP6, Eyring et al., 2016). Datasets from eight CMIP5 models and five CMIP6 models that were included in PMIP3 and PMIP4 were analysed, based on data availability via the Earth System Grid Federation (ESGF, the set of models is therefore smaller than Kageyama et al. (2021), who made use of some models only available in PMIP databases). See Table 1 for list of models with LGM simulations included in this study. Monthly surface temperature (ts), surface air temperature (tas), precipitation (pr), evapotranspiration (evspsbl) and 850 hPa wind (ua and va at 850 hPa) data from each model for a model pre-industrial control ('piControl') and LGM ('lgm') simulations were analysed. These variables were chosen to characterise the main features of LGM climate in the region and to facilitate comparison with proxy records of LGM temperature and hydroclimate. All data was re-gridded using first-order conservative remapping onto a $1.5^{\circ} \times 1.5^{\circ}$ longitude-latitude grid. Both zonal (u) and meridional (v) components of the wind were analysed, at 850 hPa except for CMIP6 INM-CM4-8 model, which only provided only near-surface (10 m) wind data for LGM simulations. PMIP3/CMIP5 and PMIP4/CMIP6 models shown in Table 1 are referred to as CMIP5 and CMIP6 models hereafter for simplification.

Deleted: s

Deleted: Section 3.2.1 of

Deleted: paper

Deleted: ¶

Deleted: our

Deleted:

Deleted: It was decided not to include CESM2-WACCM-FV2 model (Danabasoglu et al., 2020), which also performed LGM simulations due to an unrealistic climate sensitivity found by Zhu et al. (2021). Large global LGM cooling was simulated in the model, which is not consistent with proxy records and other model simulations in this study, biasing the MMM temperature results. PMIP3/CMIP5 and PMIP4/CMIP6 models shown in Table 1 are referred to as CMIP5 and CMIP6 models hereafter for simplification.¶

Deleted: ¶
Explain why used an intercomparison method, motivation for simulating the LGM, why the particular climate variables were chosen¶

Deleted: **Table 1:** List of models with models included in the study, model reference and PMIP/CMIP generation.¶
Model name ... [2]

Table 1: List of models with LGM data on NCI analysed in this study. The length of simulation years for the LGM run for each model is from Table 1 in Brown et al. (2020). The ice-sheet reconstructions are from Kageyama et al. (2021).

Model	PMIP/CMIP gen.	Lgm run length (years)	Ice-sheet reconstruction	Reference
AWI-ESM-1-1-LR	PMIP4 (CMIP6)	100	ICE-6G_C	Sidorenko et al. (2015), Lohmann et al. (2020)
CCSM4	PMIP3 (CMIP5)	101	PMIP3	Brady et al. (2013)
CESM2-WACCM-FV2	PMIP4 (CMIP6)	500	ICE-6G_C	Zhu et al. (2021)
CNRM-CM5	PMIP3 (CMIP5)	200	PMIP3	Voldoire et al. (2013)
FGOALS-g2	PMIP3 (CMIP5)	100	PMIP3	Zheng and Yu (2013)
GISS-E2-R	PMIP3 (CMIP5)	100	PMIP3	Ullman et al. (2014)
INM-CM4-8	PMIP4 (CMIP6)	200	ICE-6G_C	Volodin et al. (2018)
IPSL-CM5A-LR	PMIP3 (CMIP5)	200	PMIP3	Dufresne et al. (2013)
MIROC-ES2L	PMIP4 (CMIP6)	100	ICE-6G_C	Ohgaito et al. (2021), Hajima et al. (2020)
MIROC-ESM	PMIP3 (CMIP5)	100	PMIP3	Sueyoshi et al. (2013)
MPI-ESM-P	PMIP3 (CMIP5)	100	PMIP3	Adloff et al. (2018)
MPI-ESM1-2-LR	PMIP4 (CMIP6)	500	ICE-6G_C	Mauritsen et al. (2019)
MRI-CGCM3	PMIP3 (CMIP5)	100	PMIP3	Yukimoto et al. (2015)

The models in CMIP6 include some modifications and improvements relative to the older CMIP5 generation (Eyring et al., 2016). There are also some minor differences in the LGM experiment boundary conditions for the CMIP5 (PMIP3) and CMIP6 (PMIP4) experiments. Compared to PMIP3 experiments, new and updated boundary conditions were included in PMIP4 (as shown in Table 2), enabling the systematic analysis of the vegetation and dust forcing effects.

Furthermore, the PMIP4 protocol highlighted the specification of ice sheets, with three distinct ice sheet reconstructions available, allowing assessments of the impacts from uncertainties in ice-sheet reconstructions or boundary conditions (Kageyama et al., 2017). The PMIP3 models used PMIP3 ice-sheet configurations and the five PMIP4 models used in this study are all prescribed using the "ICE-6G_C" ice-sheet reconstruction (see Table 1). The differences between the two LGM ice-sheet reconstructions are discussed in Kageyama et al. (2017). Only CMIP6 AWI-ESM-1-1-LR model is using dynamic vegetation (https://wcrp-cmip.github.io/CMIP6_CVs/docs/CMIP6_source_id.html). The different LGM land fractions configured in each model can be seen in Supplementary Figure S1 showing the land masks for individual models.

Table 2: Summary of the main forcing or boundary conditions (experimental design) for the LGM simulations in PMIP3 and PMIP4 models (PMIP4 from Table 1 in Kageyama et al. (2017); PMIP3 from PMIP3 website: https://pmip3.lsce.ipsl.fr/). Some boundary conditions are set as the same as pre-industrial control (piControl) values.

Forcing or Boundary conditions	**PMIP4 LGM value**	**PMIP3 LGM value**
Atmospheric trace gases	CO_2 = 190 ppm CH_4 = 375 ppb N_2O = 200 ppb CFC = 0 O_3 = same as in CMIP6 *piControl*	CO_2 = 185 ppm CH_4 = 350 ppb N_2O = 200 ppb CFC = 0 O_3 = same as in CMIP5 *piControl*
Insolation	eccentricity: 0.018994 obliquity: 22.949° perihelion – 180° = 114.42°	eccentricity: 0.018994 obliquity: 22.949° perihelion – 180° = 114.42°
Ice sheets (components of model modified to represent influence of LGM ice sheet)	coastlines bathymetry ice-sheet extent altitude rivers	land-sea mask land surface elevation ocean bathymetry
Vegetation	Unless a model includes dynamic vegetation or interactive dust, the vegetation should be prescribed to be the same as in the DECK and historical runs (CMIP6 *piControl*)	as in *piControl*
Dust	as in *piControl* or *lgm* (three options)	as in *piControl*

Deleted: simulations

Deleted: ,

Deleted:

Deleted: 1

2.2 Run Length and Control Simulation

The LGM simulations are compared with pre-industrial (PI) climate as the control or baseline, similarly to many previous studies (e.g. Kageyama et al., 2021). Pre-industrial ("piControl") experiments are simulations with atmospheric composition and other boundary conditions prescribed and held constant at values representing climate before industrialization, i.e. reference year 1850 (Eyring et al., 2016). Most climate models used in this study only have 100-year length of LGM simulation based on the number of years of data available on the ESGF (refer to Table 1). According to the PMIP protocols, the models need to spin-up to equilibrium before uploading the data to ESGF (see Kageyama et al. (2017) for details of the spin-up protocol). At least 100-year data from the equilibrium part of the simulation is required to store on the ESGF (Kageyama et al., 2017). In this research, the first 100 years of output on the ESGF for each model was selected and averaged in order to capture the average climatology for each model simulation and to represent the mean state of PI and LGM climate conditions.

2.3 Classification of Australian Regions

Different regions of Australia experience different climate regimes in the present day, and are likely to respond differently to LGM climate forcing. Each region also experiences greater seasonal precipitation at a different time of year, with the north receiving most precipitation in austral summer (DJF season) and the south in austral winter (JJA season). Austral summer is the period when the Indo-Australian summer monsoon is most active, bringing precipitation to Northern Australia and nearby SH Maritime Continent areas. In austral winter, the SH westerlies shift equatorward, bringing rainfall to the Southern Australian region. We therefore divide Australia into three main regions in order to examine the LGM climate response in detail at seasonal time scales.

Shown in Figure 1, the Australian region is defined in this research bounded by longitudes from 110°E to 160°E, latitudes from 0 to 45°S. The Northern Australasia domain in the spatial plots is defined longitudes from 110°E to 160° E, and latitudes from 0 to 20°S (including New Guinea and parts of Indonesia); the Southern Australia domain is defined by longitudes from 110°E to 160°E, and latitudes from 20°S to 45°S. Lastly, the Central Australian domain is shown in the spatial plots bounded by 20°S to 35°S and 120°E to 145°E.

3 Results

3.1 Surface air temperature

In this section, the changes in surface air temperature (tas) in the LGM model simulations are evaluated in comparison with PI simulations. Figure 2 shows the simulated surface air temperature patterns from CMIP5 and CMIP6 model ensembles. No stippling is seen in Figure 2a and b indicating high model agreements in the ensembles. Despite some differences

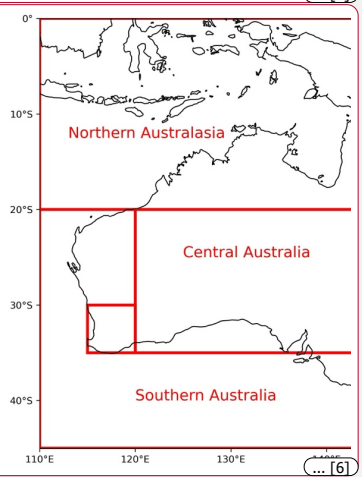

Deleted: For this research, monthly surface temperature (ts), surface air temperature (tas), precipitation (pr), evapotranspiration (evspsbl) and 850 hPa wind (ua and va at 850 hPa) data from each model for a model pre-industrial cont... [3]

Deleted: ¶

Deleted: industrialisation

Deleted: The LGM simulations from different models run for different numbers of years with a minimum length of 100 years, therefore, it is necessary to determine a uniform length of time... [4]

Deleted:

Deleted: refer to

Deleted: phase

Deleted: rom

Deleted: 2

Deleted: These three domains broadly correspond to the Tropical Australasia, Temperate Australia and Arid Interior regions discussed in Section 1.1.... [5]

Deleted: ... [6]

Deleted: S

Deleted: 3

Deleted: (excluding CMIP6 CESM2-WACCM-FV2 due to inconsistent cooling magnitude, see Figure 3),...

Deleted:

Deleted: indicate less than 70% of models

Deleted: Tthe LGM surface air temperature over Australia is warmer in the CMIP6 simulations (Figure 2b)than in thecompared to CMIP5 simulations. (Figure 2a) with high model agreements, ... [7]

between the CMIP6 and CMIP5 model simulations in LGM temperature over Australia (Figure 2c), we combine the five models from CMIP6 and the eight models from CMIP5 together into a large ensemble of thirteen models, for assessing the multi-model mean (MMM) change in temperature patterns at the LGM in this section.

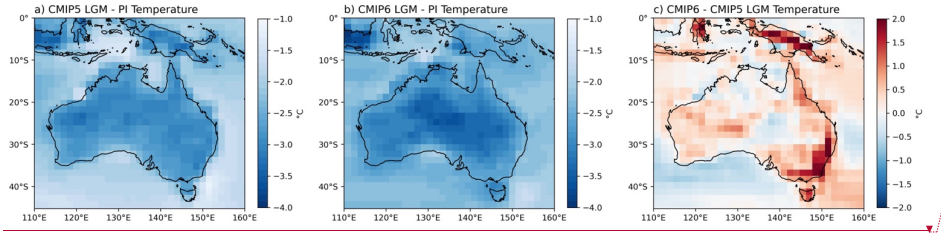

Figure 2: (a) LGM - PI mean annual surface air temperature (in °C) simulated by the ensemble of CMIP5 models, (b) LGM – PI mean annual surface temperature anomaly (in °C) simulated by CMIP6 models, (c) difference between the CMIP6 and CMIP5 LGM ensembles (in °C) over Australian region. Stippling indicates areas where less than 70% of ensemble members agree on the sign of the anomaly.

To explore the extent of model agreement for LGM surface air temperatures, Figure 3 shows the annual mean LGM - PI surface air temperature changes over Australia in individual models. All models agree on the sign of temperature change over the Australian region, with mean annual cooling during the LGM compared to PI. The cooling patterns are overall similar across most models, with more cooling over land than ocean. The MMM annual cooling averaged over Australian land areas (using modern coastlines) is -2.9 °C. Those models with greater cooling over the Australian region also tend to have greater global cooling (see Figure 5a and d). We note the much larger cooling in CMIP6 CESM2-WACCM-FV2 model is due to higher climate sensitivity of this model (Zhu et al., 2022), as seen in Figure 5d.

Deleted: (see Figure 5a, b & c for individual model differences),

Deleted: four

Deleted:

Deleted: (excludes CESM2-WACCM-FV2 model)

Deleted: 13

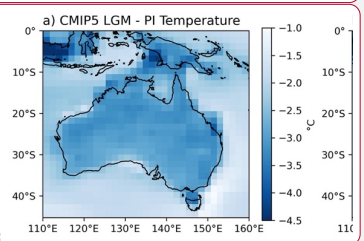

Deleted:

Deleted:

Deleted: 3

Deleted: -

Deleted: that ensemble members disagree with

Deleted: multi-model

Deleted: behaviour of individual model simulations on

Deleted: extent of model agreement on

Deleted: 4

Deleted: annual

Deleted: CMIP5 and CMIP6

Deleted: except CMIP6 CESM2-WACCM-FV2 model due to high climate sensitivity of the model (Zhu et al., 2022), …

Deleted: Northern Australia and the Maritime Continent, and more cooling over land than ocean

Deleted: 7

Deleted: CMIP5 FGOALS-g2 model simulates the strongest LGM land cooling over Australia, with an average temperature anomaly of -3.824.0 °C, compared to the MMM land average of -2.736 °C (see Table 3Figure 5a). The model differences between CMIP6 models are much smaller than between CMIP5 models (see the stippling in Figure 2a & b), possibly due to model improvements or the smaller set of models.

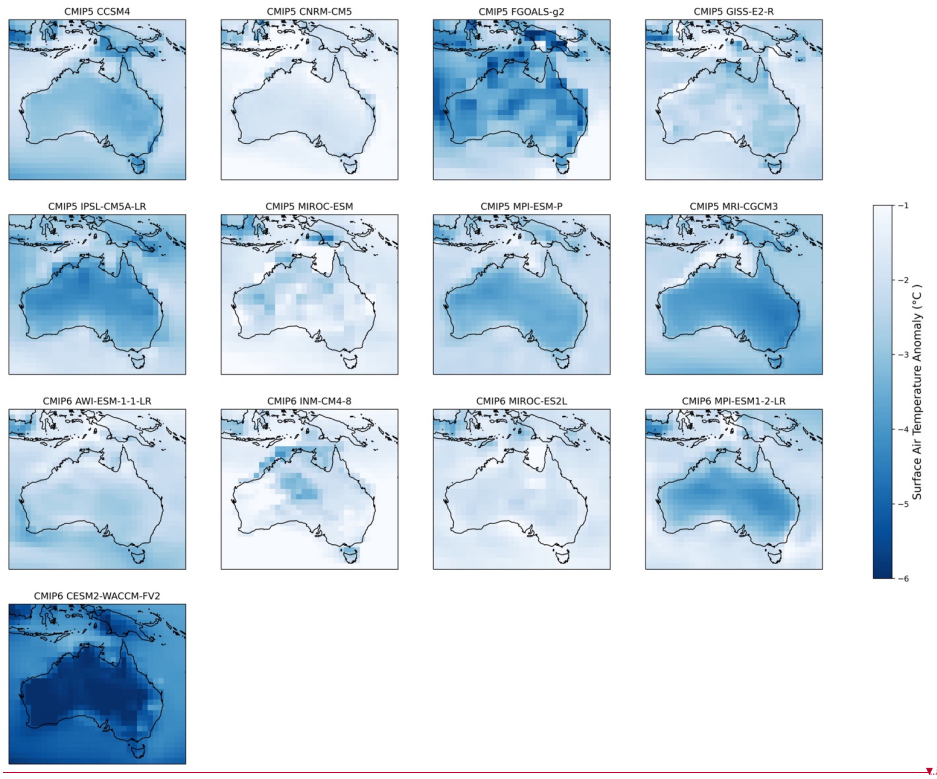

Figure 3: LGM - PI mean annual surface air temperature anomaly (°C) simulated by individual CMIP5 and CMIP6 models over Australian region.

The MMM seasonal variations in surface air temperature changes at the LGM over Australia are shown in Figure 4. The austral winter JJA season shows the strongest land average cooling (-3.1 °C, refer to Figure 5c) at the LGM, particularly along the modern coastlines in both the Northern and Southern Australian regions. LGM cooling is generally larger over land than the surrounding ocean in all seasons, with the exposed Sahul shelf area showing enhanced cooling in all seasons except SON, when there is model disagreement over the sign of the temperature anomaly over Sahul (see Figure 4d).

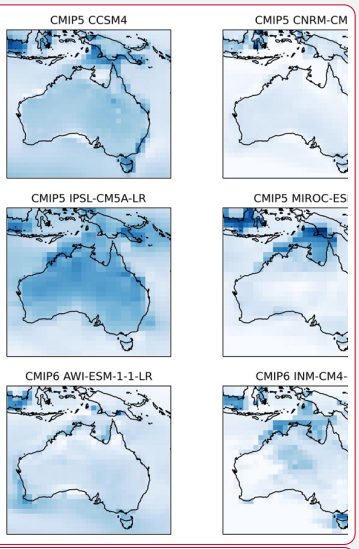

Deleted:

Deleted:

Deleted: 4

Deleted: 5

Deleted: 2.9

Deleted: Table 3

Deleted: mostly occurring

Deleted: n

Deleted: temperate

Deleted: There is more cooling over land in DJF and SON compared to JJA and MAM. The warm anomalies in DJF and SON may be due to the extension of land areas at the LGM due to lower sea level, where land areas warm more than surrounding oceans during these seasons. A similar response may also explain the coastal cooling anomalies in JJA and MAM when land cools more than ocean in these colder seasons. SST anomalies in Supplementary Figure S2.¶
Moreover, orbitally-driven changes in top of the atmosphere insolation during the LGM (see Kageyama et al., 2017) may also play a role in the seasonal differences shown in Figure 45. For the latitude range where Australia is located (~10°S to 45°S), there is an increase in insolation from January to June of 1 to 2 W/m^2 and a decrea ... [8]

Deleted: Moreover, orbitally-driven changes in top of the insolation during the LGM (see Kageyama et al., 2017) may also play a role in the seasonal differences shown in Figure 45. For the latitude range where Australia is located (~10°S to 45°S), there is an increase in insolation from January to June of 1 to 2 W/m^2 and a decrea ... [9]

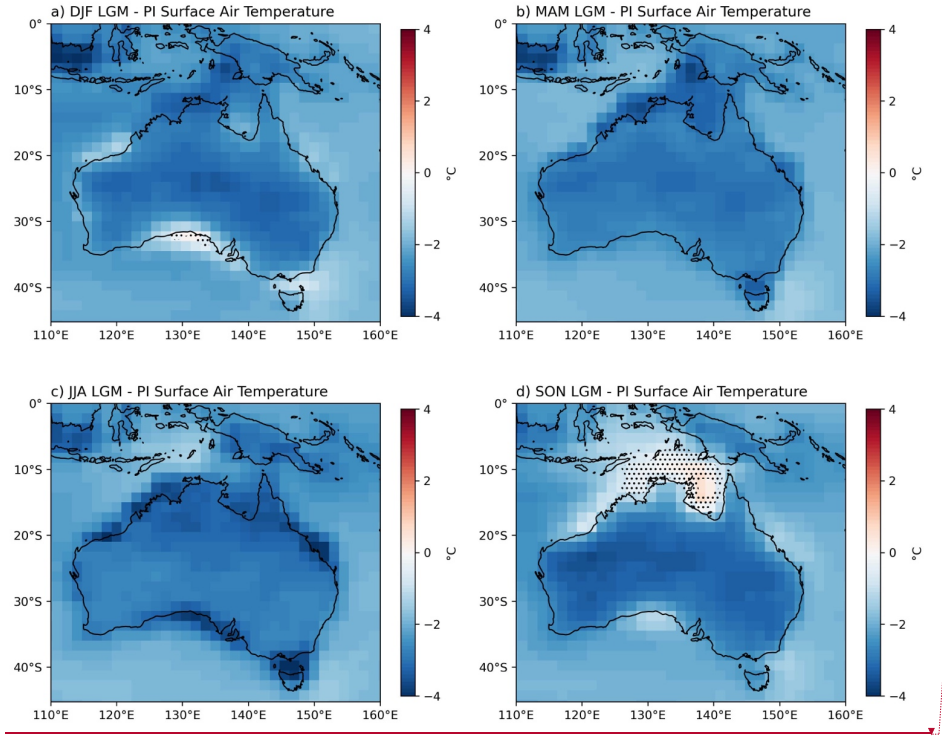

Figure 4: MMM seasonal anomalies for LGM - PI surface air temperatures (°C) simulated by the ensemble of CMIP5 and CMIP6 models for (a) DJF, (b) MAM, (c) JJA and (d) SON seasons over Australian region. Stippling indicates areas where less than 70% of ensemble members agree on the sign of the anomaly.

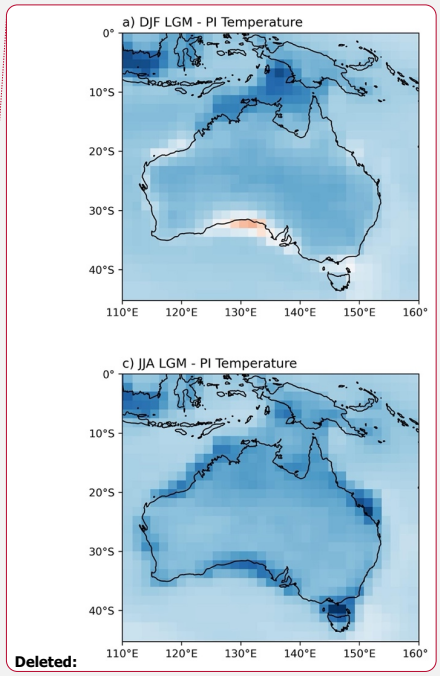

Deleted:

Deleted:

Deleted: 5

Deleted: areas where less than 70% of e

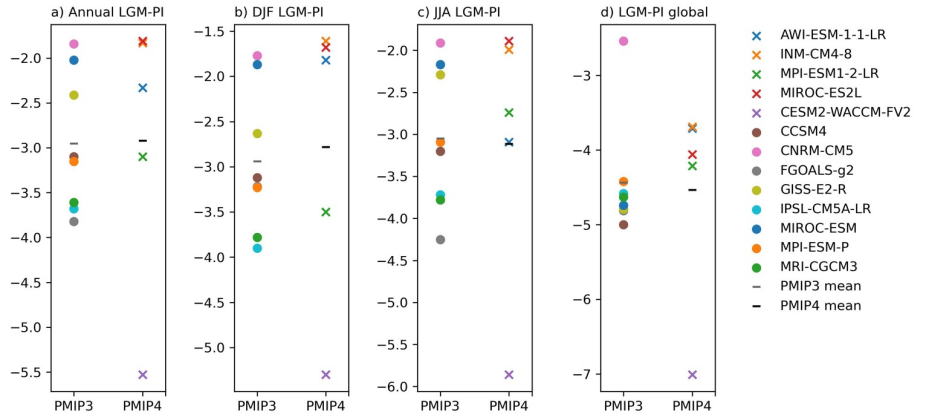

Figure 5: LGM – PI surface air temperature (tas) anomalies (°C) for (a) annual mean, (b) DJF, (c) JJA seasons over Australia (land areas within domain 0-45°S, 110°E-160°E), and (d) global annual mean surface air temperature anomalies (°C) for each CMIP5 and CMIP6 model and the multi-model mean (MMM).

3.2 Winds

This section explores the LGM - PI 850 hPa wind patterns and associated circulation changes from CMIP5/CMIP6 models over the Australian region. MMM seasonal anomalies for LGM - PI 850 hPa zonal winds and wind divergence over Australia are shown in Figure 6 (MMM excludes CMIP6 INM-CM4-8 model, with only 10 m near-surface winds available). We first consider changes over the tropical Northern Australasia domain and then focus on the temperate Southern Australia domain.

In austral summer (DJF) in the modern climate, the Indo-Australian summer monsoon is most active, with north-westerly winds and onshore moisture transport. In the LGM simulations there is a strengthening of the westerly component of the monsoon flow over Northern Australia during DJF (Figure 6a). There are regions of increased wind divergence (orange colors in Figure 6) over the Sahul shelf and parts of the expanded LGM coastline of northwest Australia, with regions of convergence or weakened divergence over adjacent ocean areas. A similar pattern of enhanced onshore westerly flow and wind convergence upstream of the Sahul shelf is seen in austral spring (SON, Figure 6d). Strengthened divergence and offshore flow is seen over this region in MAM (Figure 6c).

In austral winter (JJA) in the modern climate, the SH mid-latitude westerly winds shift northwards, allowing extratropical weather systems to influence Southern Australia. In the LGM simulations, the MMM change in JJA winds (Figure 6c) shows a weakening of the westerlies to the south of around 35°S with little change over Southern Australian land

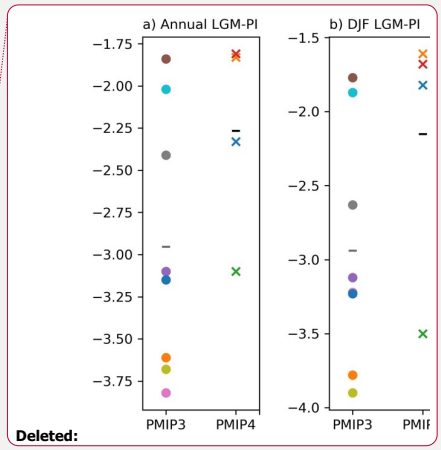

Deleted:

Deleted: s

Deleted: CCSM4 ... [10]

Deleted: 250 hPa

Deleted: LGM seasonal wind changes in austral winter (JJA season) is focused in this study, since JJA is the period when the SH westerly winds shift northwards, reaching the Southern Australian domain with increased precipitation (which will be explored in the next section). The individual model simulations of JJA wind patterns are presented in Figure 7, Figure 8 investigates the LGM meridional shifts of the SH westerlies in JJA relative to present….

areas, with the exception of a small increase in the westerly winds and wind convergence over the south-west part of this domain. Individual model simulation results are discussed next to assess the extent of model agreement in JJA season wind changes.

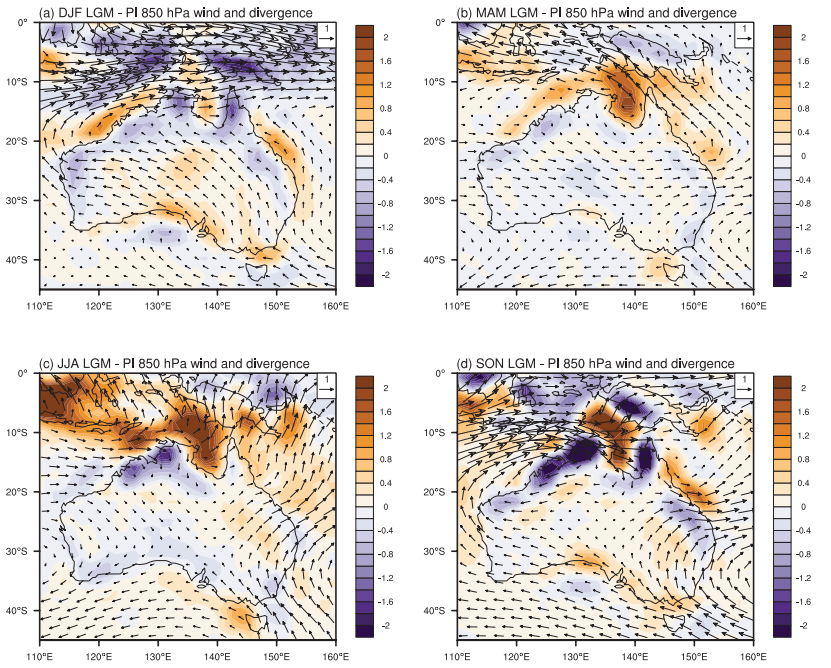

Figure 6: Seasonal average multi-model mean change (lgm – piControl) in 850 hPa winds (m/s) and wind divergence (1 x 10^{-6}/s). Wind change is shown as vectors and wind divergence change is shown as colored contours. MMM excludes INM-CM4-8 model which provided only near-surface winds.

We next investigate the meridional displacement of the SH mid-latitude westerly winds at the LGM, in comparison with previous studies (see Section 1.2), as these winds play an important role in the climate of Southern Australia (e.g. Hope et al., 2010). The LGM change in JJA winds for individual models is shown in Figure 7, with the change in the zonal component of the wind indicated as color shading. It is evident that there is large model disagreement over changes in the mid-latitude westerlies in JJA season in the Australian region. Some models show weakening and other models show

Deleted: ¶
From Figure 6, all seasons show increase in westerly zonal wind speeds in some parts of south and south-east Australian. Monsoon westerlies strengthen in DJF to the north of Australia, while easterlies strengthen south of around 15°S. JJA season shows very different patterns for zonal winds at 850 hPa, with stronger westerlies to the south of around 35°S and weaker westerlies north of this latitude. In JJA season, some regions in northern tropical Australasia and eastern Australia are dominated by meridional wind changes (Figure 6c). The northward anomaly over Northern Australia and the Maritime continent may be linked to stronger cross-equatorial flow during SH winter. In austral summer (DJF season), the Indo-Australian summer monsoon is most active, which brings precipitation to northern Australia and nearby Maritime Continent areas. From Figure 6a, it seems that the westerly component of this wind is strengthened, extending to the western Pacific region during the LGM. The winds over surrounding ocean areas weakened, yet there seems to be enhanced, anti-cyclonic circulation within Australian mainland areas at the LGM in DJF. I

Deleted: I.

Deleted:

Deleted: 3.2.1 Shifts of the westerlies¶

Deleted: are interested in

Deleted: ing

Deleted: s

Deleted: T

Deleted: and also at a hemispheric and global scale (not shown)

strengthening in the region to the south of Australia, with a slight weakening of the MMM westerly wind south of around 35°S as discussed above (see Figure 6).

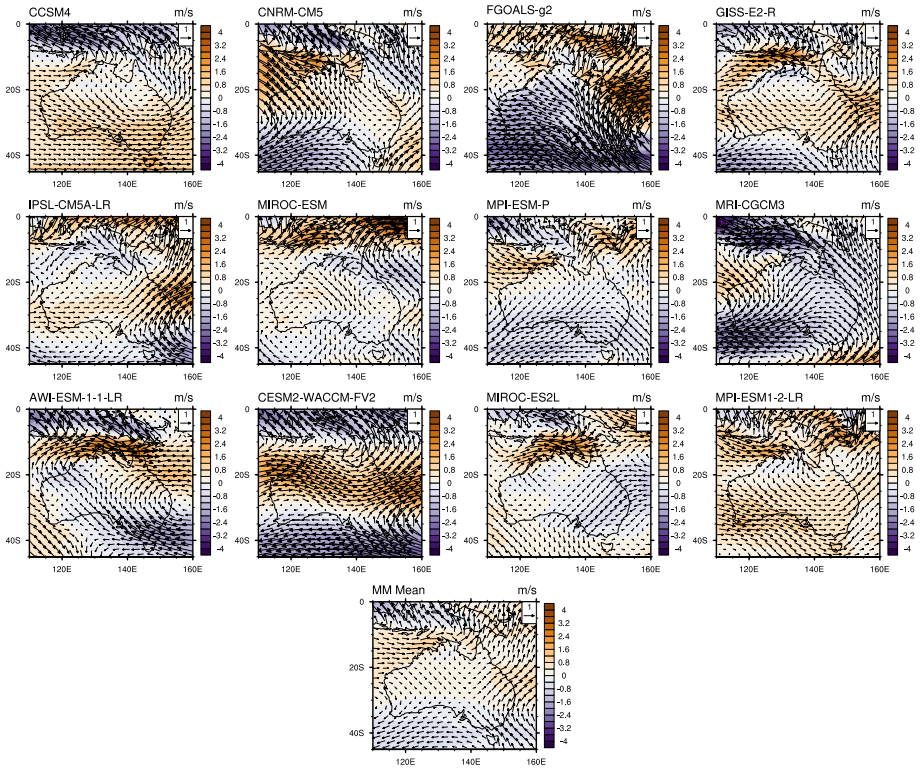

Figure 7: Change in JJA 850 hPa winds (lgm – piControl) for each model and multi-model mean over the Australian domains. Wind change is shown as vectors and zonal (westerly) wind change is shown as colored contours (m/s).

To further investigate shifts in the position of SH westerly winds or changes in their intensity, the zonal-mean zonal wind is plotted over the SH tropics and midlatitudes. Figure 8 shows the zonal-mean 850 hPa zonal winds in JJA over SH (0-

Deleted: little change in

Moved down [1]: To further investigate shifts in the extent of SH westerly winds or changes in their intensity, the zonal-mean zonal wind is plotted over the SH tropics and midlatitudes. Figure 8 shows the zonal-mean 850 hPa zonal winds in JJA over SH (0-70ºS).¶

Deleted: 7

Moved (insertion) [1]

Deleted: We are interested in investigating the meridional displacement of the SH mid-latitude westerly winds at the LGM, in comparison with previous studies (see Section 1.2), as these winds play an important role in the climate of southern Australia (e.g. Hope et al., 2010). There is large model disagreement over changes in the westerlies in both JJA (Supplementary Figure S1) and Annual (not shown) in the Australian region and also at a hemispheric and global scale (not shown). Some models show weakening and other models show strengthening in the region to the south of Australia, with little change in the MMM. To further investigate shifts in the extent of SH westerly winds or changes in their intensity, the zonal-mean zonal wind is plotted over the SH tropics and midlatitudes. Figure 6 shows the zonal-mean 850 hPa zonal winds in JJA over SH (0-70ºS).¶

Deleted: extent

70ºS). The majority of models do not show clear evidence of latitudinal changes for maximum mid-latitude zonal wind speed at the LGM compared to PI, with some disagreements between models (see Figure 8). There is a weak equatorward shift in maximum zonal wind speed seen in IPSL-CM5A-LR and MIROC-ESM models. However, there also seems to be opposite poleward shifts of the maximum zonal winds in CCSM4, FGOALS-g2 and MRI-CGCM3 models. Most models except CCSM4 and MRI-CGCM3 models show overall weakening of SH mid-latitude westerlies at the LGM compared to PI.

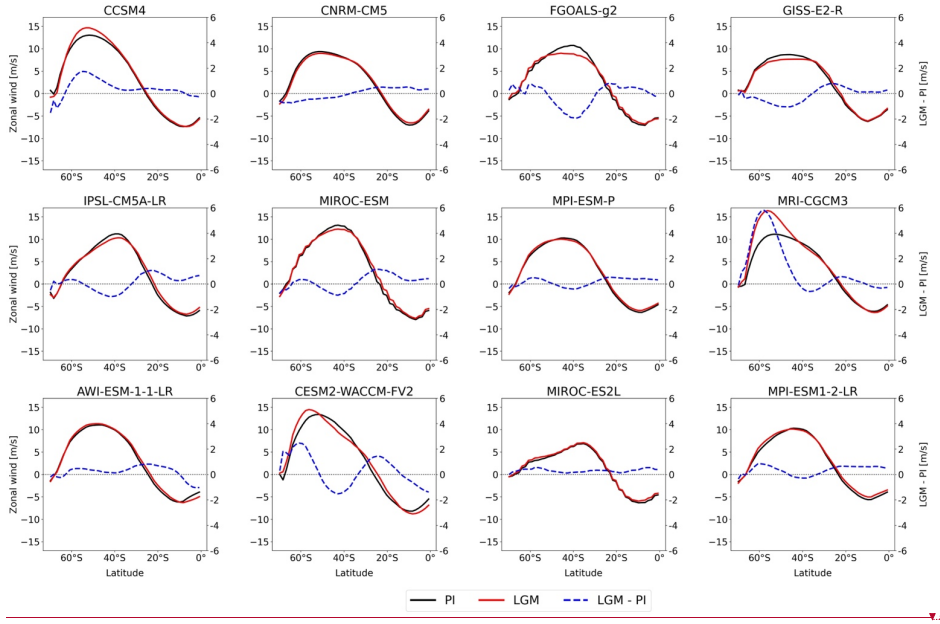

Figure 8: JJA Zonal-mean zonal wind (m/s) at 850 hPa simulated by individual CMIP5 and CMIP6 models (except INM-CM4-8 model which provided only near-surface winds) for SH (0 to 70ºS). PI in black colour and LGM in red colour, blue dashed line is LGM anomalies (LGM - PI). The LGM - PI zonal wind anomaly (m/s) for each model is displayed on a secondary y-axis. Zonal mean is calculated over all longitudes.

Deleted: ¶

Deleted: ,

Deleted: and there are

Deleted: 6

Deleted: ost

Deleted: The latitudinal positions of the boundary lines between SH westerlies and easterlies (i.e. latitude of zero zonal wind) for each CMIP5 and CMIP6 model in JJA season for both PI and LGM simulations are also calculated over the Australian domain (110ºE to 160ºE), values are given in Table 4. All models except FGOALS-g2 model show a positive (equatorward) shift for the boundary lines at the LGM relative to PI, even for the models with poleward shifted maximum zonal winds (e.g. CCSM4 and MRI-CGCM3, as stated earlier). CMIP5 FGOALS-g2 model simulated a poleward (negative) shift in both the latitudinal positions for the boundary lines and its SH maximum zonal winds. The two models that simulated relatively large displacement of boundary lines (CNRM-CM5, GISS-E2-R models) show no change in their maximum zonal winds (see Figure 6). ¶

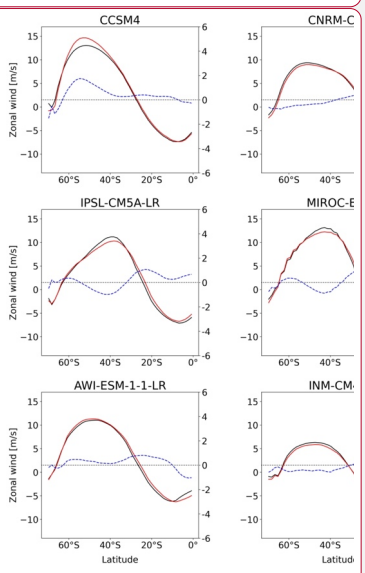

Deleted:

Deleted:

Deleted: 6

3.3 Precipitation

As noted in Section 3.2, in the present-day climate, regional precipitation variations over Australia are associated with seasonal variations in atmospheric circulation. Austral summer (DJF season) is the period when the Indo-Australian summer monsoon is most active, bringing precipitation to northern Australia and nearby Maritime Continent areas. In austral winter (JJA season), the SH westerlies shift equatorward, bringing precipitation to Southern Australia. This section examines the LGM changes in precipitation and moisture balance over the Australian region relative to PI with a focus on seasonal anomalies. The model agreement is also considered.

The LGM - PI annual average precipitation anomalies over Australia for each model are shown in Figure 9. It is evident that the largest model precipitation anomalies occur over Northern Australasia, due to the higher absolute precipitation totals in the tropics. Some models (e.g. GISS-E2-R and INM-CM4-8) simulate increased annual average precipitation over the Sahul shelf region whereas most of the other models show drier conditions. Most models agree on an annual mean decreased precipitation at the LGM averaged over the Australia mainland (see Table 3), however, regional increases in precipitation are also simulated by most models, indicating that thermodynamic reductions in LGM precipitation due to cooling may be offset by dynamical increases at regional scales. Individual model precipitation changes in the DJF and JJA seasons are shown in Supplementary Figures S2 and S3, also displaying model disagreement over tropical regions in DJF but widespread drying in most models in JJA.

Deleted: Table 4: Latitudes of zero westerly wind speed (westerly-easterly boundary) for each CMIP5 and CMIP6 model in JJA season (INM-CM4-8 model used near-surface winds). Calculations were over the Australian domains from 110ºE to 160ºE.¶
Model name ... [11]

Deleted: I

Deleted: rainfall

Deleted: the s

Deleted: n region

Deleted: e

Deleted: aims to

Deleted: are therefore discussed

Deleted: for each model

Deleted: 7

Deleted: from Figure 97

Deleted: northern Australia and the Maritime Continen

Deleted: t

Deleted:

Deleted: Larger model disagreement over northern Australia may be due to the different changes in SST and atmospheric circulations simulated in each model in this region, where model precipitation is highly sensitive to SST gradients (e.g. Chadwick et al., 2013) (see Supplementary Figure S2 for MMM annual mean SST change at the LGM over a larger domain extending across the Pacific and Indian Oceans). …

Deleted: in the tropical monsoon

Deleted: 2

Deleted: 3

Deleted: .

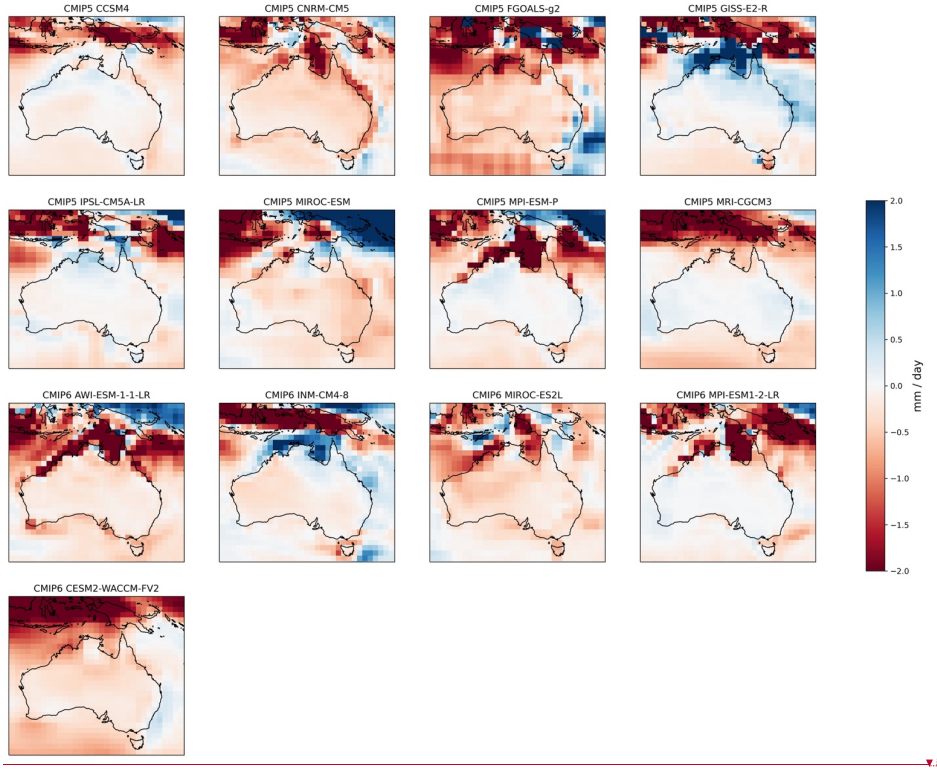

Figure 9: LGM – PI mean annual precipitation anomaly (mm/day) simulated by individual CMIP5 and CMIP6 models over the Australian domains.

MMM seasonal precipitation anomalies from the combined CMIP5 and CMIP6 model ensemble at the LGM over Australia are shown in Figure 10 and seasonal precipitation changes over specific domains are summarised in Table 3. Stippling denotes regions where less than 70% of ensemble members agree on the sign of the anomaly. In austral summer (DJF) season, an increase in precipitation can be seen over parts of Northern Australasia, particularly the central northern Australian region, while other regions become drier (Figure 10a). Most parts of Australia become drier in MAM, with the strongest drying over the Sahul shelf and Maritime Continent, indicating an earlier monsoon retreat (Figure 10b).

Deleted:

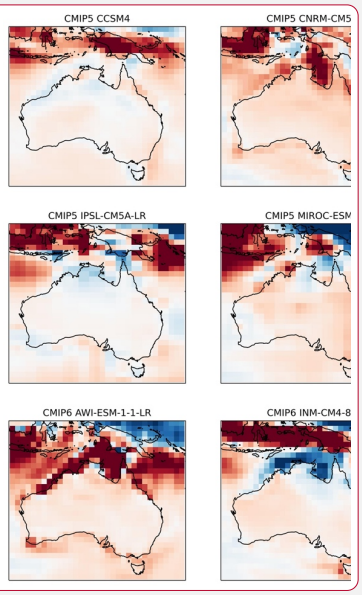

Deleted:

Deleted: 7

Deleted: 8

Deleted: 5

Deleted: (seasonal precipitation evapotranspiration anomaly comparisons between CMIP5 and CMIP6 models is presented in Supplementary Figure S54)…

Deleted: that

Deleted: dis

Deleted: with 70% multi-model

Deleted: sign

Austral winter (JJA) season shows the strongest area-average land drying (-0.59 mm/day) over Australia (0-45°S, 110°E-160°E) during the LGM (Figure 10c). There is a strong precipitation reduction over northern Australia and the Maritime Continent in JJA, consistent with previous analysis of PMIP3 LGM simulations (Yan et al., 2018). The south-western corner of Australia shows an average increase in precipitation in JJA but with low model agreement (Figure 10c). There is a strong increase in precipitation in SON, with high model agreement, over the exposed Sahul shelf and central northern Australia (Figure 10d), as well as along the east coast. This is also consistent with Yan et al. (2018), who identified increased Australian monsoon precipitation in early austral summer (November-December) in PMIP3 LGM simulations.

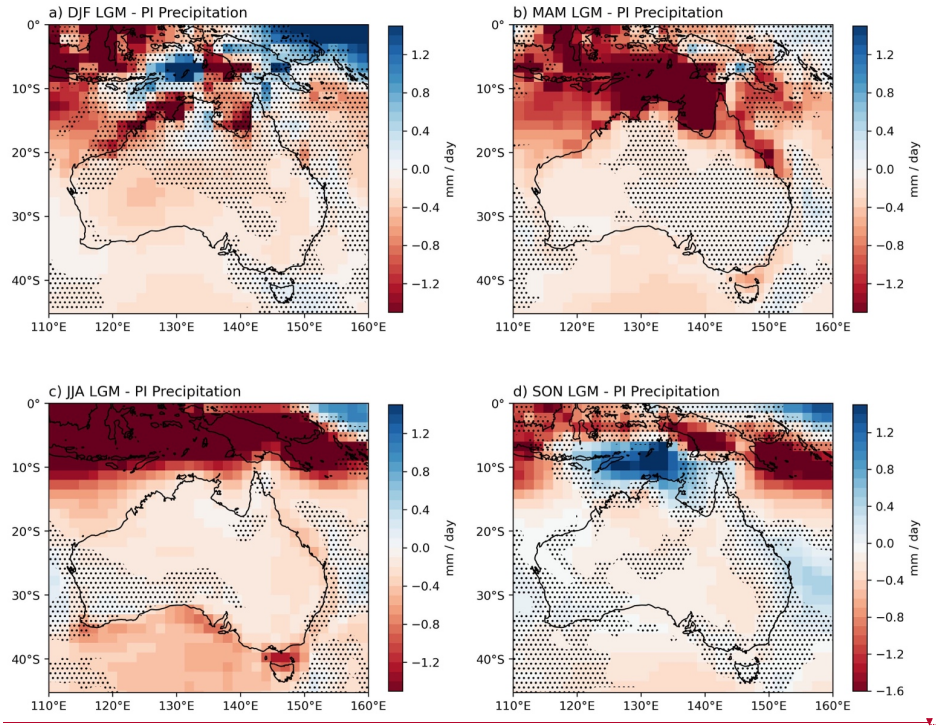

Figure 10: MMM seasonal anomalies for LGM – PI precipitation (mm/day) simulated by the ensemble of CMIP5 and CMIP6 models for (a) DJF, (b) MAM, (c) JJA and (d) SON seasons over Australian region. Stippling indicates areas where less than 70% of ensemble members agree on the sign of the anomaly.

Deleted: , dominated by the

Deleted: s

Deleted: 8

Deleted: In austral summer (DJF) season, an increase in precipitation can be seen over parts of northern Australasia, particularly the central "Top End"northern Australian region, while other regions become drier (Figure 108a). In S

Deleted: In SON t

Deleted: , however we do not find a clear increase in DJF based on the models examined here. Most parts of Australia become drier in

Deleted: Most parts of Australia become drier in MAM, whereas there is a strong increase in precipitation in the tropical north-west (including over the Sahul shelf) and along the east coast in SON. …

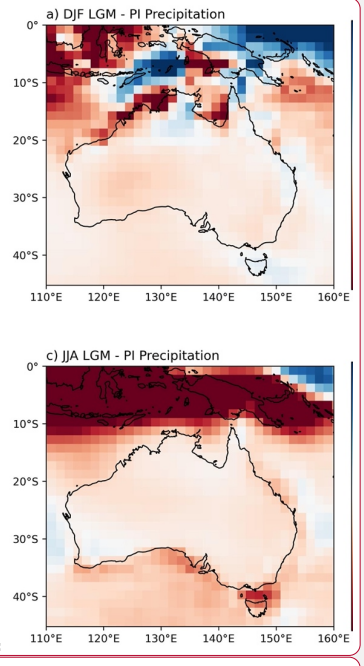

Deleted:

Deleted:

Deleted: 8

3.3.1 Precipitation minus evapotranspiration (P-E)

As some proxy records provide information about available moisture or effective precipitation changes at the LGM relative to PI, instead of direct evidence for precipitation changes (e.g. Petherick et al., 2013; Sniderman et al., 2019; Fitzsimmons et al., 2012), we also examine changes in the moisture balance or P-E (precipitation minus evapotranspiration) in the LGM simulations. Cooler conditions at the LGM may lead to reduced evaporation and hence a positive P-E despite reduced precipitation (e.g. Scheff et al., 2017; Kageyama et al., 2021).

Annual mean LGM precipitation and evapotranspiration changes over the Australian regions are shown in Figure 11a and b while net precipitation (P-E) is shown in Figure 11c (seasonal mean evapotranspiration changes are shown in Supplementary Figure S4). There is an annual mean reduction in precipitation during the LGM across the Australian mainland, New Guinea and parts of the Maritime Continent, with an annual average land precipitation change of -0.3 mm/day (based on PI land mask, so excluding coastal areas which are land in the LGM only). The strong precipitation reductions simulated in the expanded land areas in the Northern Australasia region and also the exposed Bass Strait region are associated with decreased evaporation rates at the LGM, so that overall increased LGM P-E was simulated (Figure 11). Changes in both precipitation and P-E averaged over different land domains are given in Table 3.

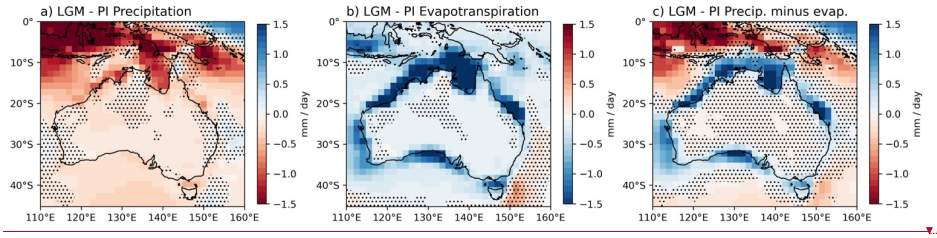

Figure 11: LGM – PI mean annual (a) precipitation (b) evapotranspiration and (b) P-E (in mm/day) simulated by the ensemble of CMIP5 and CMIP6 models over Australian region. Stippling indicates areas where less than 70% of ensemble members agree on the sign of the anomaly.

Figure 12 shows the LGM seasonal variations in net precipitation (P-E) over Australia, which can be compared with the seasonal changes in precipitation shown in Figure 10. In comparison to the variable precipitation pattern at the LGM (Figure 10), the P-E pattern (Figure 12) provides more seasonally consistent spatial changes over Australia during the LGM with the largest increase in P-E over the expanded land areas at the LGM. It is also important to note that model disagreement over the sign of the P-E change is large due to the small magnitude of the changes inland from coastal areas.

Deleted: 9
Deleted: and
Deleted: 9
Deleted: 9
Deleted: xxx
Deleted: northern tropical
Deleted: monsoon
Deleted: 9
Deleted: 5
Deleted: a) LGM - PI Precipitation
Deleted:
Deleted:
Deleted: 9
Deleted: 0
Deleted: 8
Deleted: 8
Deleted: 0
Deleted: M
Deleted: s are also larger

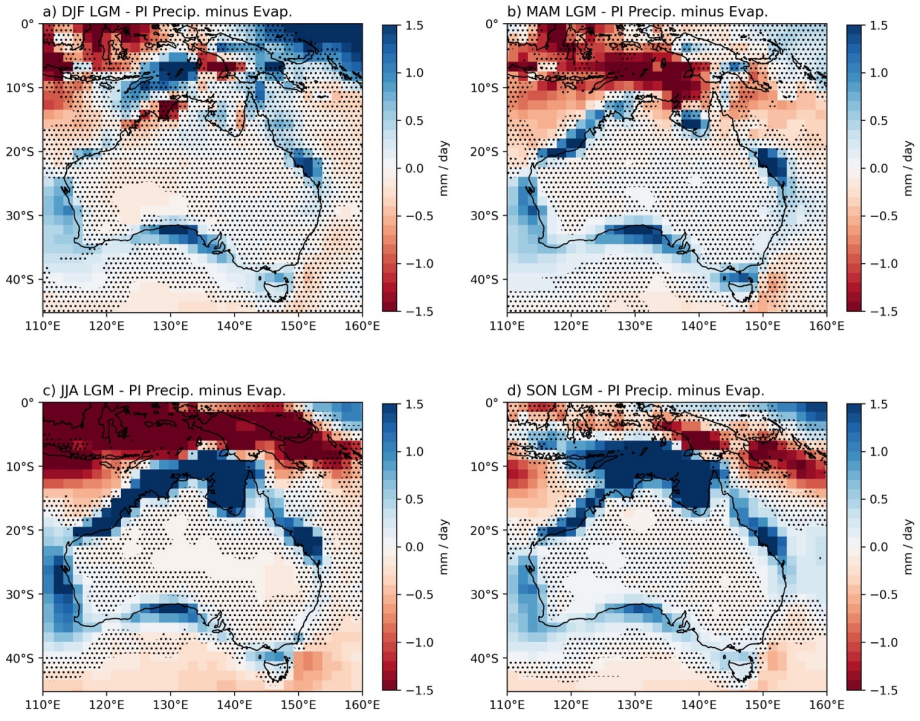

Figure 12: MMM seasonal anomalies for LGM – PI precipitation-evapotranspiration (P-E, mm/day) simulated by the ensemble of CMIP5 and CMIP6 models for (a) DJF, (b) MAM, (c) JJA and (d) SON seasons over Australian region. This can be compared with MMM seasonal precipitation shown in Figure 10 and MMM seasonal evapotranspiration shown in Supplementary Figure S4. Stippling indicates areas where less than 70% of ensemble members agree on the sign of the anomaly.

Table 3 shows the average land precipitation and P-E changes at the LGM in individual models over Northern Australasia in DJF and Southern Australia in JJA and the annual mean anomalies over the mainland Australian area south of 10°S, excluding the Maritime Continent. The Australian mainland region experienced an increase in P-E simulated in all models, with a MMM P-E increase of 0.14 mm/day (Table 3). Individual model simulations of annual average LGM P-E changes are shown in Supplementary Figure S5.

In the Northern Australasia domain, most models show consistent DJF drier conditions in both average LGM precipitation and P-E changes, although large model disagreements occur (see DJF P-E changes in individual models in

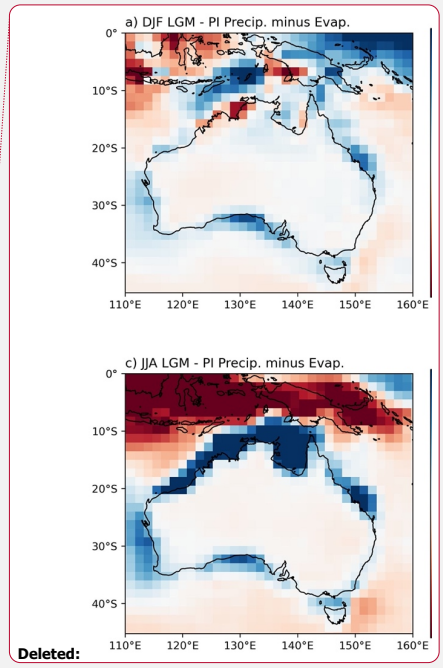

Deleted:

Deleted: **1210…** MMM seasonal anomalies for LGM – P… [12]

Deleted: 5

Deleted: northern

Deleted: (0-20°S, 110°E-160°E)

Deleted: season

Deleted: southern Australia (20°S-45°S, 110°E-160°E; see… [13]

Deleted: whole domain

Deleted: The Australian mainland region experienced an increase in P-E simulated in all models, with a MMM P-E increase of 0.14 mm/day (Table 35). …

Deleted: can be seen

Deleted: 5

Supplementary Figure S6). All models except GISS-E2-R simulated more positive P-E anomalies compared to the corresponding LGM precipitation change. In the Southern Australia region, all models agree on reduced JJA area-average precipitation (see individual model simulations in Supplementary Figure S3) and positive P-E anomalies at the LGM, with the exception of FGOALS-g2 model which has a very small negative JJA P-E anomaly (-0.05 mm/day) (Table 3). Mean P-E changes at the LGM in JJA season for each model over the Australian domain are shown in Supplementary Figure S7. Overall, it is evident that the LGM changes in P-E are less negative (DJF) or positive (JJA and annual average) compared with negative precipitation changes for the MMM and many of the individual models.

Table 3: Average land precipitation and P-E LGM anomalies (mm/day) over Northern Australasia (0-20°S, 110°E-160°E) in DJF season. JJA land averages over Southern Australia (20°S-45°S, 110°E-160°E). Annual mean land average changes for modern Australia mainland (10°S-45°S, 110°E-160°E, excluding Maritime Continent) for each CMIP5 and CMIP6 model and MMM. Land is defined by PI land mask.

Model name	DJF average over Northern Australasia land (mm/day)		JJA average over Southern Australia land (mm/day)		Annual average over modern Australia mainland (mm/day)	
	Precipitation	P - E	Precipitation	P - E	Precipitation	P - E
AWI-ESM-1-1-LR	-0.85	-0.64	-0.25	0.06	-0.38	0.00
CCSM4	-0.48	-0.24	-0.20	0.03	-0.06	0.18
CESM2-WACCM-FV2	-1.88	-1.47	-0.29	0.01	-0.30	0.16
CNRM-CM5	-0.63	-0.12	-0.15	0.19	-0.38	0.10
FGOALS-g2	-0.58	-0.14	-0.70	-0.05	-0.44	0.04
GISS-E2-R	1.02	0.70	-0.14	0.06	0.18	0.31
INM-CM4-8	-0.19	0.18	-0.07	0.21	-0.06	0.22
IPSL-CM5A-LR	1.10	1.17	-0.19	0.10	0.04	0.28
MIROC-ES2L	-0.85	-0.39	-0.19	0.11	-0.37	0.05
MIROC-ESM	0.53	0.74	-0.26	0.10	-0.27	0.11
MPI-ESM-P	-0.83	-0.20	-0.03	0.10	-0.12	0.05
MPI-ESM1-2-LR	-0.61	-0.25	-0.03	0.11	-0.08	0.08
MRI-CGCM3	-1.23	-0.86	-0.04	0.25	0.00	0.30
MMM	-0.42	-0.12	-0.20	0.10	-0.17	0.14

Deleted: 6
Deleted: 3
Deleted: ‘
Deleted: ’
Deleted: that
Deleted: was simulated
Deleted: 5
Deleted: 7
Deleted:
Deleted: 2
Deleted: -0.30
Deleted: -0.01
Deleted: -0.19
Deleted: 0.11
Deleted: -0.16
Deleted: 0.14

3.3.2 Drivers of precipitation change

LGM cooling is likely to lead to overall drier conditions due to the thermodynamic response (a colder atmosphere holds less moisture), as seen in the annual mean MMM change (Figure 2). However, the models do not simulate drying over all regions or in all seasons over Australia. For instance, annually wetter conditions are found over the south-west of Australia and parts of the tropics in some models (Figure 9) and regions of increased MMM precipitation are found over the tropics in DJF and SON (Figures 10). While a decomposition of thermodynamic and dynamic components of precipitation change is not included in this study, it is evident that the thermodynamic drying response is dominant over much of the Australian land area in the individual models and the seasonal MMM precipitation changes.

Over the Northern Australasia domain, the seasonal precipitation changes are complex and not clearly linked to temperature changes over either land or ocean. However, changes in temperature gradients between land and ocean may be important in driving circulation change (see Supplementary Figure S8 for annual surface temperature changes over Northern Australia in each model with different LGM land mask configurations shown in Supplementary Figure S1). The exposure of the Sahul shelf appears to drive changes in moisture transport, with increased onshore westerlies (Figure 6) driving convergence upstream of the LGM coastline, producing increased precipitation to the northwest of Australia over a small region in DJF (Figure 10a) and a larger region in SON (Figure 10d). The disagreement in simulated austral summer precipitation between models (Supplementary Figure S2) can also be linked to different changes in circulation in the models (not shown). Offshore wind anomalies and increased wind divergence in MAM and JJA produces widespread drying over the entire Northern Australasia region. Further analysis of moisture convergence fields is required to confirm this mechanism, but it is broadly consistent with the findings of Yan et al. (2018) based on PMIP3 LGM simulations.

LGM precipitation changes over Southern Australia appear to be dominated by thermodynamic drying, with additional contributions from dynamical processes including shifts in the position or intensity of the SH mid-latitude westerlies. While area average precipitation changes over the Southern Australia domain are negative in JJA, the majority of models simulate increased precipitation over the south-west corner of Southern Australia (see Supplementary Figure S3). This region is also climatically distinct in the modern climate, experiencing higher winter rainfall than surrounding areas, with a recent strong drying trend (Hope et al. 2010).

We explored the relationship between the JJA LGM change in precipitation averaged over south-west Australia (30ºS-35ºS, 115ºE-120ºE) and the change in strength of the westerly winds over the same latitude range, but with a wider longitude range for the entire Southern Australian region (110°E-155°E). The corresponding scatter plot is shown in Supplementary Figure S9. The Pearson correlation coefficient between the two variables is r = 0.52, and the corresponding p-value is 0.081, indicating that the correlation is not significant at the 95% confidence level. Sime et al. (2013) found that there is no clear relationship between the displacements of westerlies and enhanced precipitation at the LGM based on PMIP models, which is consistent with our findings. However, the positive anomalies in the south-west indicate a dynamical driver of precipitation increase is stronger than thermodynamic drying in this region.

Deleted: 4

Deleted: 7

Deleted: ¶

Deleted:)

Deleted: The relationships between temperature and precipitation changes at the LGM compared to PI are evaluated over the monsoon-affected Northern Australasia domain in this section as temperature and precipitation patterns may be closely related in the tropics (e.g. Chadwick et al., 2013). Figure 45 shows the MMM seasonal changes for surface air temperature and Figure 108 shows the MMM seasonal changes for precipitation during the LGM. Wetter conditions are found to the north of Australia in SON and DJF (Figure 108), possibly in response to changes in seasonal heating over the exposed continental shelf or changes in atmospheric circulation. ¶
The cooling anomalies over Northern Australasia in MAM season (Figure 45b) appear to correspond to the strong drying anomalies in the same region (Figure 108b). However, the opposite relationship can also be seen. In DJF season, both increased and decreased precipitation is simulated over Northern Australasia (Figure 108a), however, reduction in temperature is seen across the whole region (Figure 45a). Similarly, warming anomalies are found over the central southern coastlines in DJF and SON (Figure 45a, d), while no large changes in precipitation are seen over the same region (Figure 108a, d). Thus, there is no simple linear relationship between regional patterns of LGM temperature and precipitation change.¶
3.3.2.21 Winds¶
We now investigate the drivers of LGM precipitation patterns in southern Australia by examining the correlation between precipitation in the south-west of Australia and SH mid-latitude westerlies in JJA, since they shift equatorward in this season, bringing moisture mainly via frontal systems to this area in the present-day climate (Hope et al., 2010). The analysis focuses on a smaller south-west box rather than the larger southern Australia domain as there is a larger increase in precipitation in the LGM evident in the south-west region in many models. …

Deleted: ¶
Figure 11 shows the

Deleted: ; see Figure 2

Deleted: 5

Deleted: 2

Deleted: a moderate positive correlation between the two variables

Deleted: . This suggests that larger westerly wind speeds are likely to be associated with enhanced precipitation in this region. The wind and temperature anomaly values for each model are listed in Table S1 in the Supplement.¶

Deleted: proposed

Deleted: . While we also find no clear relationship over the SH or Southern Australia scale, over the south-west Australian corner we do find a moderate correlation between westerly wind strength and precipitation changes over south-west Australia at the LGM.…

4 Discussion and Conclusions

This study has evaluated the temperature, precipitation and wind changes over the Australian region at the LGM compared with pre-industrial conditions from CMIP5 and CMIP6 model simulations. We now summarise the key finding from the model simulations and briefly compare these with published proxy records of LGM temperature, precipitation and atmospheric circulation from this region, introduced in Section 1.

4.1 Temperature

The LGM ensemble of thirteen CMIP5 and CMIP6 models simulates a global annual cooling of surface air temperature of -4.5 ºC compared to PI conditions, within the range proposed in other modelling studies (e.g. Annan et al., 2022; Tierney et al., 2020a). Regionally, the models simulate cooling of annual surface air temperatures in the range of -1.8 ºC to -5.5 ºC (MMM = -2.9 ºC) in the Australian domain (0-45°S, 110°E-160°E), with larger cooling over land and particularly over coastal regions with expanded land area at the LGM. On seasonal time scales, cooling is slightly larger in MAM and JJA over this region. Our model results for temperature change generally agree well with available proxy records and previous modelling studies although there are some LGM proxy records that imply greater LGM cooling than the models. For example, Miller et al. (1997) and Hope (2009) reconstructed greater cooling over land than was simulated by the models, with Miller et al. (1997) finding cooling of 9 ºC in inland Australia and Hope (2009) finding cooling of 4-6 ºC in the New Guinea highlands. This may be due to uncertainties in the proxy reconstruction. Alternatively, the models may not be simulating the extent of cooling over land in the LGM simulations. In the case of proxy records over high topography (e.g. Hope, 2009), the models also may not have resolved the details of the topography and associated cooling.

4.2 Precipitation

The models simulate an overall reduced precipitation over the Australian region, with negative annual average anomalies in the majority of models and the MMM. Seasonal MMM precipitation anomalies (Figure 10) indicate widespread, slightly lower precipitation than today, except for slightly higher precipitation during DJF, in the north-eastern central Northern Australia, northern Cape York, and all of Tasmania except the west coast; during JJA in SW western Australia; and during SON in the subtropical eastern margin of the continent. Examination of the P-E patterns (Figure 12) shows most of the continent experienced reduced precipitation but positive P-E anomalies, implying that most regions at the LGM would have experienced little change in moisture availability, or slightly wetter conditions, particularly on seasonal time scales.

Some paleoclimate proxies (e.g. Fitzsimmons et al., 2013; Petherick et al., 2013; Cadd et al., 2018; Rowe et al., 2021) have been interpreted as indicating substantially lower LGM moisture availability, which is not consistent with the changes in P-E from the PMIP/CMIP simulations analysed in this study. On the other hand, studies of paleo-river channels near the Murray-Darling Basin indicate that relatively high fluvial discharge, and thus moisture availability, were maintained at the LGM (e.g. Cohen et al., 2015; Kemp et al., 2017; Treble et al., 2017; Hesse et al., 2018). The contradiction between

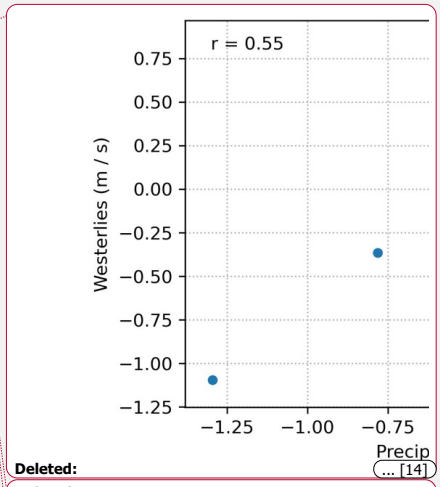

Deleted: ... [14]
Deleted: to
Deleted: based on
Deleted: s
Deleted: 13
Deleted: T
Deleted: regional
Deleted: 4.0
Deleted: 6
Deleted: which do not show good agreements with
Deleted: show
Deleted: also
Deleted: not
Deleted: We also tested whether using surface air temperature ("tas") from models provided a better match with proxy reco ... [15]
Deleted: 8
Deleted: WA
Deleted: 0
Deleted: do not show obviously intensified wetness of any of the higher precipitation regions. In turn, the central Northern Au ... [16]
Deleted: negative
Deleted: and
Deleted: most regions would have experienced LGM hydroclimatic stasis (i.e. little change in moisture availability) or slightly w ... [17]
Deleted: in

some proxy reconstructions and model simulations may reflect the fact that vegetation-based hydroclimate reconstructions have not taken into account the effects of low atmospheric CO_2 on plant growth, which is increasingly recognised as a factor that should not be ignored (Prentice et al., 2017; Scheff et al., 2017; Sniderman et al., 2019). Moreover, it is increasingly suspected (e.g. Scheff et al., 2017; Roderick et al., 2015) that greater LGM dustiness and dune-mobilisation are secondary effects from reduced plant productivity, via landscape destabilisation. Alternatively, the large model disagreement suggests that at least some models are not realistically simulating the LGM hydroclimate response in this region. The reasons for this are beyond the scope of the present study, but likely reflect biases in model convection, land surface interactions or other relevant processes.

4.3 Winds

Similar to many previous studies, we did not find a consistent equatorward or poleward shift in the SH mid-latitude westerly winds at the LGM over the Australian longitude range or a wider SH zonal average (not shown) based on the available CMIP5 and CMIP6 model simulations. Over the south-west corner of Southern Australia, increased LGM precipitation in austral winter (JJA) was more likely in models with strengthened SH westerlies over the surrounding domain, although the correlation was not significant. However, we did not identify a consistent shift in maximum SH mid-latitude zonal winds in the LGM simulations.

4.4 Conclusions

This research presents an initial evaluation and analysis of climate conditions (temperature, precipitation, wind) over the Australian domain (including adjacent regions of Indonesia and New Guinea) at the LGM using an ensemble of eight CMIP5 and five CMIP6 models with available PMIP LGM simulations. The results offer insights into regional Australian climate variations during the LGM, and the inter-connections between climate variables in different seasons. Our model results show widespread cooling in the annual mean and all seasons, with a magnitude that is generally consistent with available proxy records except in central Australia and high elevations in New Guinea, where models show less cooling than proxy records.

The models disagree on changes in precipitation over Northern Australasia in austral summer, with a complex multi-model mean pattern of precipitation change. The lack of model agreement indicates that each model responds differently to the specified changes in boundary conditions at the LGM, producing different changes in circulation and therefore different dynamical components of the precipitation response. This implies that caution is required when comparing proxy records with simulations from a single model or small group of models in this tropical region. Uncertainty in both model simulations and the interpretation of proxy records of hydroclimate limits quantitative model-proxy comparisons.

In Southern Australia, the changes in precipitation indicate widespread drying over land in all seasons, except for the southwest of the continent. The changes in the position or intensity of the SH westerlies are not consistent between

Deleted: partly

Deleted: problem

Deleted: In brief, C3 plants perceive an LGM world with low (180 ppm) CO_2, as much 'drier' than today, so that model simulations with dynamic vegetation typically show widespread forest reduction, even when holding temperature and precipitation at modern values. …

Deleted: other

Deleted: this study

Deleted: Focusing on the Australian sector, this study tried to detect changes in the latitude of the SH westerly winds in austral winter (JJA) through investigating the position of the boundary lines between westerly and easterly winds for each model. From our calculations of their latitudinal positions at the LGM and PI, most models agree on an equatorward shift at the LGM with a multi-model average displacement of 0.65° northwards. However, we did not

Deleted: . Future work could conduct additional evaluations such as examining upper-level winds (as in Kageyama et al., 2021), or use a larger ensemble of models and more comprehensive dynamical analysis to address this question.¶

Deleted: for the

Deleted: a wider

Deleted: the

Deleted: twelve

Deleted: 8

Deleted: 5

Deleted: Previously, few studies using coupled model simulations of LGM climate have focused on this region or even the Southern Hemisphere. The results offer insights into some

Deleted: some

Deleted: generally agree with published proxy records and other model studies, with some exceptions as discussed in Section 4.show

Deleted: ¶

models, again suggesting that caution is required when comparing simulations from a single model with proxy records from this region. Given the large changes in global and regional temperature in the LGM simulations, with similar patterns of cooling in all models, it is noteworthy that the models do not simulate a consistent shift in this important component of the regional circulation, suggesting that shifts in the position of the westerlies cannot be assumed as a simple response to large-scale climate cooling (or warming).

Further analysis is required to better understand the divergent model responses to LGM boundary conditions in both the tropics and mid-latitudes in the Australian region. This analysis may also provide guidance for understanding model responses in a future warming climate. Comparison with well constrained proxy records of past hydroclimate changes would also provide a useful target for identifying more realistic model simulations. Such comparison will need to consider the moisture balance rather than focusing only on precipitation, and will need to account for sensitivity of some proxies to changes in CO_2 levels.

Deleted: Several analyses were also conducted in this study to assess the relationships between westerly winds and precipitation, and temperature and precipitation. A moderate positive correlation between the JJA westerlies and precipitation over south-west Australia (30ºS-35ºS) was found, indicating larger westerly wind speeds with enhanced precipitation. In contrast, no clear relationship between surface temperature and precipitation changes is found in this study, which leaves future work to further investigate drivers of regional LGM precipitation change.¶

Code and data availability

The CMIP5 and CMIP6 model data used in this study are available from the Earth System Grid Federation.

Supplement

The Supplement related to this article is available online at:

Author contributions

YD and JRB designed the study. YD carried out the data analysis and led the writing of the manuscript. JRB and JMKS provided comments on the results and contributed to the writing of the manuscript.

Competing interests

The authors declare that they have no conflict of interest.

Acknowledgments

Josephine R. Brown and Yanxuan Du acknowledge support from the Australian Research Council Centre of Excellence for Climate Extremes (CE170100023). We acknowledge the World Climate Research Programme, which, through its Working Group on Coupled Modelling, coordinated and promoted CMIP6. We thank the climate modelling groups for producing and making available their model output, the Earth System Grid Federation (ESGF) for archiving the data and providing access,

and the multiple funding agencies who support CMIP6 and ESGF. CMIP5 and CMIP6 model outputs were made available with the assistance of resources from the National Computational Infrastructure (NCI), which is supported by the Australian government.

References

Adloff, M., Reick, C. H., and Claussen, M.: Earth system model simulations show different feedback strengths of the terrestrial carbon cycle under glacial and interglacial conditions, Earth Syst. Dynam., 9, 413–425, https://doi.org/10.5194/esd-9-413- 2018, 2018.

Annan, J. D. and Hargreaves, J. C.: A new global reconstruction of temperature changes at the Last Glacial Maximum, Clim. Past, 9, 367–376, https://doi.org/10.5194/cp-9-367-2013, 2013.

Annan, J. D., Hargreaves, J. C., and Mauritsen, T.: A new global surface temperature reconstruction for the Last Glacial Maximum, Clim. Past, 18, 1883–1896, https://doi.org/10.5194/cp-18-1883-2022, 2022.

Bird, M. I., O'Grady, D., and Ulm, S.: Humans, water, and the colonization of Australia, Proc. Natl. Acad. Sci. U.S.A., 113, 11477-11482, https://doi.org/10.1073/pnas.1608470113, 2016.

Braconnot, P., Harrison, S. P., Kageyama, M., Bartlein, P. J., Masson-Delmotte, V., Abe-Ouchi, A., Otto-Bliesner, B., and Zhao, Y.: Evaluation of climate models using palaeoclimatic data, Nat. Clim. Change, 2, 417-424, https://doi.org/10.1038/nclimate1456, 2012.

Bradshaw, C. J. A., Norman, K., Ulm, S., Williams, A. N., Clarkson, C., Chadœuf, J., Lin, S. C., Jacobs, Z., Roberts, R. G., Bird, M. I., Weyrich, L. S., Haberle, S. G., O'Connor, S., Llamas, B., Cohen, T. J., Friedrich, T., Veth, P., Leavesley, M., and Saltré, F.: Stochastic models support rapid peopling of Late Pleistocene Sahul, Nat. Commun., 12, 2440, https://doi.org/10.1038/s41467-021-21551-3, 2021.

Brady, E. C., Otto-Bliesner, B. L., Kay, J. E., and Rosenbloom, N.: Sensitivity to Glacial Forcing in the CCSM4, J. Climate, 26, 1901–1925, https://doi.org/10.1175/JCLI-D-11-00416.1, 2013.

Brown, J. R., Brierley, C. M., An, S. I., Guarino, M. V., Stevenson, S., Williams, C. J. R., Zhang, Q., Zhao, A., Abe-Ouchi, A., Braconnot, P., Brady, E. C., Chandan, D., D'Agostino, R., Guo, C., LeGrande, A. N., Lohmann, G., Morozova, P. A., Ohgaito, R., O' ishi, R., Otto-Bliesner, B. L., Peltier, W. R., Shi, X., Sime, L., Volodin, E. M., Zhang, Z., and Zheng, W.:

Deleted:

Deleted: Proceedings of the National Academy of Sciences

Deleted: 10.1073/pnas.1608470113

Deleted: ure

Deleted: ications

Deleted: 10.1038/s41467-021-21551-3

Comparison of past and future simulations of ENSO in CMIP5/PMIP3 and CMIP6/PMIP4 models, Clim. Past, 16, 1777-1805, https://doi.org/10.5194/cp-16-1777-2020, 2020.

Byrne, M.: Evidence for multiple refugia at different time scales during Pleistocene climatic oscillations in southern Australia inferred from phylogeography, Quaternary Sci. Rev., 27, 2576-2585, https://doi.org/10.1016/j.quascirev.2008.08.032, 2008.

Cadd, H. R., Tibby, J., Barr, C., Tyler, J., Unger, L., Leng, M. J., Marshall, J. C., McGregor, G., Lewis, R., Arnold, L. J., Lewis, T., and Baldock, J.: Development of a southern hemisphere subtropical wetland (Welsby Lagoon, south-east Queensland, Australia) through the last glacial cycle, Quaternary Sci. Rev., 202, 53-65, https://doi.org/10.1016/j.quascirev.2018.09.010, 2018.

Cadd, H., Petherick, L., Tyler, J., Herbert, A., Cohen, T., Sniderman, K., Barrows, T. T., Fulop, R. T., Knight, J., Kershaw, A. P., Colhoun, E. A., and Harris, M.: A continental perspective on the timing of environmental change during the last glacial stage in Australia, Quaternary Res., 102, 5-23, https://doi.org/10.1017/qua.2021.16, 2021.

Chadwick, R., Boutle, I., and Martin, G.: Spatial patterns of precipitation change in CMIP5: Why the rich do not get richer in the tropics, J. Climate, 26, 3803-3822, https://doi.org/10.1175/JCLI-D-12-00543.1, 2013.

Chavaillaz, Y., Codron, F., and Kageyama, M.: Southern westerlies in LGM and future (RCP4.5) climates, Clim. Past, 9, 517-524, https://doi.org/10.5194/cp-9-517-2013, 2013.

Clark, P. U., Dyke, A. S., Shakun, J. D., Carlson, A. E., Clark, J., Wohlfarth, B., Mitrovica, J. X., Hostetler, S. W., and McCabe, A. M.: The Last Glacial Maximum, Science, 325, 710–714, https://doi.org/10.1126/science.1172873, 2009.

Clarkson, C., Jacobs, Z., Marwick, B., Fullagar, R., Wallis, L., Smith, M., Roberts, R. G., Hayes, E., Lowe, K., Carah, X., Florin, S. A., McNeil, J., Cox, D., Arnold, L. J., Hua, Q., Huntley, J., Brand, H. E. A., Manne, T., Fairbairn, A., Shulmeister, J., Lyle, L., Salinas, M., Page, M., Connell, K., Park, G., Norman, K., Murphy, T., and Pardoe, C.: Human occupation of northern Australia by 65,000 years ago, Nature, 547, 306, https://doi.org/10.1038/nature22968, 2017.

Cohen, T.J., John, D. J., Luke, A. G., Joshua, R. L., Gerald, C. N., Jan-Hendrik, M., Brian, G. J., and David, M. P.: Hydrological transformation coincided with megafaunal extinction in central Australia, Geology, 43, 195–198, https://doi.org/10.1130/G36346.1, 2015.

Deleted: ence
Deleted: iews
Deleted: 10.1016/j.quascirev.2008.08.032
Deleted: &
Deleted: &
Deleted: Jansen
Deleted: Gliganic
Deleted: Larsen
Deleted: Nanson
Deleted: May
Deleted: Jones
Deleted: Price
Deleted: ;
Deleted: .
Deleted: (3)
Deleted: :
Deleted: . doi:

Danabasoglu, G., Lamarque, J.-F., Bacmeister, J., Bailey, D. A., DuVivier, A. K., Edwards, J., Emmons, L. K., Fasullo, J., Garcia, R., Gettelman, A., Hannay, C., Holland, M. M., Large, W. G., Lauritzen, P. H., Lawrence, D. M., Lenaerts, J. T. M., Lindsay, K., Lipscomb, W. H., Mills, M. J., Neale, R., Oleson, K. W., Otto-Bliesner, B., Phillips, A. S., Sacks, W., Tilmes, S., van Kampenhout, L., Vertenstein, M., Bertini, A., Dennis, J., Deser, C., Fischer, C., Fox-Kemper, B., Kay, J. E., Kinnison, D., Kushner, P. J., Larson, V. E., Long, M. C., Mickelson, S., Moore, J. K., Nienhouse, E., Polvani, L., Rasch, P. J., and Strand, W. G.: The Community Earth System Model Version 2 (CESM2), J. Adv. Model. Earth Syst., 12, e2019MS001916, https://doi.org/10.1029/2019MS001916, 2020.

Denniston, R. F., Wyrwoll, K. H., Asmerom, Y., Polyak, V. J., Humphreys, W. F., Cugley, J., Woods, D., LaPointe, Z., Peota, J., and Greaves, E.: North Atlantic forcing of millennial-scale Indo-Australian monsoon dynamics during the Last Glacial period, Quaternary Sci. Rev., 72, 159-168, https://doi.org/10.1016/j.quascirev.2013.04.012, 2013.

De Deckker, P., Moros, M., Perner, K., Blanz, T., Wacker, L., Schneider, R., Barrows, T. T., O' Loingsign, T., and Jansen, E.: Climatic evolution in the Australian region over the last 94 ka - spanning human occupancy -, and unveiling the Last Glacial Maximum, Quaternary Sci. Rev., 249, https://doi.org/10.1016/j.quascirev.2020.106593, 2020.

DiNezio, P. N., and Tierney, J. E.: The effect of sea level on glacial Indo-Pacific climate, Nat. Geosci., 6, 485-491, https://doi.org/10.1038/NGEO1823, 2013.

Dufresne, J. L., Foujols, M. A., Denvil, S., Caubel, A., Marti, O., Aumont, O., Balkanski, Y., Bekki, S., Bellenger, H., Benshila, R., Bony, S., Bopp, L., Braconnot, P., Brockmann, P., Cadule, P., Cheruy, F., Codron, F., Cozic, A., Cugnet, D., de, Noblet, N., Duvel, J. P., Ethé, C., Fairhead, L., Fichefet, T., Flavoni, S., Friedlingstein, P., Grandpeix, J. Y., Guez, L., Guilyardi, E., Hauglustaine, D., Hourdin, F., Idelkadi, A., Ghattas, J., Joussaume, S., Kageyama, M., Krinner, G., Labetoulle, S., Lahellec, A., Lefebvre, M. P., Lefevre, F., Levy, C., Li, Z. X., Lloyd, J., Lott, F., Madec, G., Mancip, M., Marchand, M., Masson, S., Meurdesoif, Y., Mignot, J., Musat, I., Parouty, S., Polcher, J., Rio, C., Schulz, M., Swingedouw, D., Szopa, S., Talandier, C., Terray, P., Viovy, N., and Vuichard, N.: Climate change projections using the IPSL-CM5 Earth System Model: from CMIP3 to CMIP5, Clim. Dynam., 40, 2123–2165, https://doi.org/10.1007/s00382-012-1636-1, 2013.

Ehlers, J., and Gibbard, P. L.: The extent and chronology of Cenozoic Global Glaciation, Quat. Int., 164-165, 6-20, https://doi.org/10.1016/j.quaint.2006.10.008, 2007.

Eyring, V., Bony, S., Meehl, G. A., Senior, C. A., Stevens, B., Stouffer, R. J., and Taylor, K. E.: Overview of the Coupled Model Intercomparison Project Phase 6 (CMIP6) experimental design and organization, Geosci. Model Dev., 9, 1937–1958, https://doi.org/10.5194/gmd-9-1937-2016, 2016.

Deleted: Denniston, R. F., Asmerom, Y., Lachniet, M., Polyak, V. J., Hope, P., An, N., Rodzinyak, K., and Humphreys, W. F.: A Last Glacial Maximum through middle Holocene stalagmite record of coastal Western Australia climate, Quaternary Sci. Rev., 77, 101-112, https://doi.org/10.1016/j.quascirev.2013.07.002, 2013. …

Fitzsimmons, K. E., Cohen, T. J., Hesse, P. P., Jansen, J., Nanson, G. C., May, J.-H., Barrows, T. T., Haberlah, D., Hilgers, A., Kelly, T., Larsen, J., Lomax, J., and Treble, P.: Late Quaternary palaeoenvironmental change in the Australian drylands, Quaternary Sci. Rev., 74, 78-96, https://doi.org/10.1016/j.quascirev.2012.09.007, 2013.

Fitzsimmons, K. E., Miller, G. H., Spooner, N. A., and Magee, J. W.: Aridity in the monsoon zone as indicated by desert dune formation in the Gregory Lakes basin, northwestern Australia, Aust. J. Earth Sci., 59, 469-478, https://doi.org/10.1080/08120099.2012.686171, 2012.

Hajima, T., Watanabe, M., Yamamoto, A., Tatebe, H., Noguchi, M. A., Abe, M., Ohgaito, R., Ito, A., Yamazaki, D., Okajima, H., Ito, A., Takata, K., Ogochi, K., Watanabe, S., and Kawamiya, M.: Development of the MIROC-ES2L Earth system model and the evaluation of biogeochemical processes and feedbacks, Geosci. Model Dev., 13, 2197–2244, https://doi.org/10.5194/gmd-13- 2197-2020, 2020.

Hesse, P. P., Williams, R., Ralph, T. J., Frirs, K. A., Larkin, Z. T., Westaway, K. E., and Farebrother, W.: Palaeohydrology of lowland rivers in the Murray-Darling Basin, Australia, Quaternary Sci. Rev., 200, 85-105, https://doi.org/10.1016/j.quascirev.2018.09.035, 2018.

Holden, P. B., Edwards, N. R., Oliver, K. I. C., Lenton, T. M., and Wilkinson, R. D.: A probabilistic calibration of climate sensitivity and terrestrial carbon change in GENIE-1, Clim. Dynam., 35, 785, https://doi.org/10.1007/s00382-009-0630-8, 2010.

Hope, G.: Environmental change and fire in the Owen Stanley Ranges, Papua New Guinea, Quaternary Sci. Rev., 28, 2261-2276, https://doi.org/10.1016/j.quascirev.2009.04.012, 2009.

Hope, P: The Weather and Climate of Australia at the Last Glacial Maximum, PhD Thesis, University of Melbourne, School of Earth Sciences, 2005.

Hope, P., Timbal, B., and Fawcett, R.: Associations between rainfall variability in the southwest and southeast of Australia and their evolution through time, Int. J. Climatol., 30, 1360-1371, https://doi.org/10.1002/joc.1964, 2010.

Hughes, P. D., Gibbard, P. L., and Ehlers, J.: Timing of glaciation during the last glacial cycle: evaluating the concept of a global 'Last Glacial Maximum' (LGM), Earth-Sci Rev., 125, 198–171, https://doi.org/10.1016/j.earscirev.2013.07.003, 2013.

Deleted: &

Jungclaus, J., Mikolajewicz, U., Kapsch, M.-L., D'Agostino, R., Wieners, K.-H., Giorgetta, M., Reick, C., Esch, M., Bittner, M., Legutke, S., Schupfner, M., Wachsmann, F., Gayler, V., Haak, H., de Vrese, P., Raddatz, T., Mauritsen, T., von Storch, J.-S., Behrens, J., Brovkin, V., Claussen, M., Crueger, T., Fast, I., Fiedler, S., Hagemann, S., Hohenegger, C., Jahns, T., Kloster, S., Kinne, S., Lasslop, G., Kornblueh, L., Marotzke, J., Matei, D., Meraner, K., Modali, K., Müller, W., Nabel, J., Notz, D., Peters, K., Pincus, R., Pohlmann, H., Pongratz, J., Rast, S., Schmidt, H., Schnur, R., Schulzweida, U., Six, K., Stevens, B., Voigt, A., and Roeckner, E.: MPI-M MPI-ESM1.2-LR model output prepared for CMIP6 PMIP lgm, Version 20190710, Earth System Grid Federation, https://doi.org/10.22033/ESGF/CMIP6.6642, 2019.

Kageyama, M., Albani, S., Braconnot, P., Harrison, S. P., Hopcroft, P. O., Ivanovic, R. F., Lambert, F., Marti, O., Peltier, W. R., Peterschmitt, J.-Y., Roche, D. M., Tarasov, L., Xu Zhang, Brady, E. C., Haywood, A. M., LeGrande, A. N., Lunt, D. J., Mahowald, N. M., Mikolajewicz, U., and Nisancioglu, K. H.: The PMIP4 contribution to CMIP6 - Part 4: Scientific objectives and experimental design of the PMIP4-CMIP6 Last Glacial Maximum experiments and PMIP4 sensitivity experiments, Geosci. Model Dev., 10, 4035–4055, https://doi.org/10.5194/gmd-10-4035-2017, 2017.

Kageyama, M., Braconnot, P., Harrison, S. P., Haywood, A. M., Jungclaus, J. H., Otto-Bliesner, B. L., Peterschmitt, J.-Y., Abe-Ouchi, A., Albani, S., Bartlein, P. J., Brierley, C., Crucifix, M., Dolan, A., Fernandez-Donado, L., Fischer, H., Hopcroft, P. O., Ivanovic, R. F., Lambert, F., Lunt, D. J., Mahowald, N. M., Peltier, W. R., Phipps, S. J., Roche, D. M., Schmidt, G. A., Tarasov, L., Valdes, P. J., Zhang, Q., and Zhou, T.: The PMIP4 contribution to CMIP6 – Part 1: Overview and over-arching analysis plan, Geosci. Model Dev., 11, 1033–1057, https://doi.org/10.5194/gmd-11-1033-2018, 2018.

Kageyama, M., Harrison, S. P., Kapsch, M.-L., Lofverstrom, M., Lora, J. M., Mikolajewicz, U., Sherriff-Tadano, S., Vadsaria, T., Abe-Ouchi, A., Bouttes, N., Chandan, D., Gregoire, L. J., Ivanovic, R. F., Izumi, K., LeGrande, A. N., Lhardy, F., Lohmann, G., Morozova, P. A., Ohgaito, R., Paul, A., Peltier, W. R., Poulsen, C. J., Quiquet, A., Roche, D. M., Shi, X., Tierney, J. E., Valdes, P. J., Volodin, E., and Zhu, J.: The PMIP4 Last Glacial Maximum experiments: preliminary results and comparison with the PMIP3 simulations, Clim. Past, 17, 1065–1089, https://doi.org/10.5194/cp-17-1065-2021, 2021.

Kemp, J., Pietsch, T., Gontz, A., and Olley, J: Lacustrine-fluvial interactions in Australia's Riverine Plains, Quaternar Sci. Rev., 166, 352-362, https://doi.org/10.1016/j.quascirev.2017.02.015, 2017.

Kim, S. J., Flato, G., and Boer, G.: A coupled climate model simulation of the Last Glacial Maximum, Part 2: approach to equilibrium, Clim. Dynam., 20, 635-661, https://doi.org/10.1007/s00382-002-0292-2, 2003.

Deleted: &

Kitoh, A., Murakami, S., and Koide, H.: A simulation of the Last Glacial Maximum with a coupled atmosphere-ocean GCM, 28, 2221-2224, https://doi.org/10.1029/2000GL012271, 2001.

Kohfeld, K. E., Graham, R. M., de Boer, A. M., Sime, L. C., Wolff, E. W., Le Quéré, C., and Bopp, L.: Southern Hemisphere westerly wind changes during the Last Glacial Maximum: paleo-data synthesis, Quaternary Sci. Rev., 68, 76-95, https://doi.org/10.1016/j.quascirev.2013.01.017, 2013.

Lambeck, K., Rouby, H., Purcell, A., Sun, Y., and Sambridge, M.: Sea level and global ice volumes from the Last Glacial Maximum to the Holocene, Proc. Natl. Acad. Sci. U.S.A., 111, 15296–15303, https://doi.org/10.1073/pnas.1411762111, 2014.

Lamy, F., Gersonde, R., Winckler, G., Esper, O., Jaeschke, A., Kuhn, G., Ullermann, J., Martinez-Garcia, A., Lambert, F., and Kilian, R.: Increased Dust Deposition in the Pacific Southern Ocean During Glacial Periods, Science, 343, 404–407, https://doi.org/10.1126/science.l245424, 2014.

Liu, Z., Lu, Z., Wen, X., Otto-Bliesner, B. L., Timmermann, A., and Cobb, K. M.: Evolution and forcing mechanisms of El Niño over the past 21,000 years, Nature, 515, 550-553, https://doi.org/10.1038/nature13963, 2014.

Liu, S., Jiang, D., and Lang, X.: The Weakening and Eastward Movement of ENSO Impacts during the Last Glacial Maximum, J. Climate, 33, 5507-5526, https://doi.org/10.1175/JCLI-D-19-0728.1, 2020.

Marshall, A. G., and Lynch, A. H.: Time-slice analysis of the Australian summer monsoon during the late Quaternary using the Fast Ocean Atmosphere Model, J. Quat. Sci., 21, 789-801, https://doi.org/10.1002/jqs.1063, 2006.

Miller, G. H., Magee, J. W., and Jull, A. J. T.: Low-latitude glacial cooling in the Southern Hemisphere from amino-acid racemization in emu eggshells, Nature, 385, 241-244, https://doi.org/10.1038/385241a0, 1997.

Nevill, P. G., Bossinger, G., and Ades, P. K.: Phylogeography of the world's tallest angiosperm, Eucalyptus regnans: evidence for multiple isolated Quaternary refugia, J. Biogeogr., 37, 179-192, https://doi.org/10.1111/j.1365-2699.2009.02193.x, 2010.

Newnham, R. M., Lowe, D. J., Giles, T., and Alloway, B. V.: Vegetation and climate of Auckland, New Zealand, since ca. 32 000 cal. yr ago: Support for an extended LGM, J. Quat. Sci., 22, 517–534, https://doi.org/10.1002/jqs.1137, 2007.

Deleted: ¶

Moved (insertion) [2]

Moved up [2]: Marshall, A. G., & Lynch, A. H. (2006). Time-slice analysis of the Australian summer monsoon during the late Quaternary using the Fast Ocean Atmosphere Model. *Journal of Quaternary Science*, *21*(7), 789-801.¶

Deleted: ournal of

Deleted: aphy

Ohgaito, R., Yamamoto, A., Hajima, T., O'ishi, R., Abe, M., Tatebe, H., Abe-Ouchi, A., and Kawamiya, M.: PMIP4 experiments us- ing MIROC-ES2L Earth system model, Geosci. Model Dev., 14, 1195–1217, https://doi.org/10.5194/gmd-14-1195-2021, 2021.

Otto-Bliesner, B. L., Brady, E. C., Clauzet, G., Tomas, R., Levis, S., and Kothavala, Z.: Last Glacial Maximum and Holocene Climate in CCSM3, J. Climate, 9, 2526-2544, https://doi.org/10.1175/JCLI3748.1, 2006.

Pepper, M. and Keogh, J. S.: Life in the "dead heart" of Australia: The geohistory of the Australian deserts and its impact on genetic diversity of arid zone lizards, J. Biogeogr., 48, 716-746, https://doi.org/10.1111/jbi.14063, 2021.

Petherick, L., Bostock, H., Cohen, T. J., Fitzsimmons, K., Tibby, J., Fletcher, M. S., Moss, P., Reeves, J., Monney, S., Barrows, T., Kemp, J., Jansen, J., Nanson, G., and Dosseto, A.: Climatic records over the past 30 ka from temperate Australia – a synthesis from the Oz-INTIMATE workgroup, Quaternary Sci. Rev., 74, 58-77, https://doi.org/10.1016/j.quascirev.2012.12.012, 2013.

Prentice, I. C., Cleator, S. F., Huang, Y. H., Harrison, S. P., and Roulstone, I.: Reconstructing ice-age palaeoclimates: Quantifying low-CO2 effects on plants, Glob. Planet. Change., 149, 166–176, https://doi.org/10.1016/j.gloplacha.2016.12.012, 2017.

Prentice, I. C., Harrison, S. P., and Bartlein, P. J.: Global vegetation and terrestrial carbon cycle changes after the last ice age, New Phytol., 189, 988–998, https://doi.org/10.1111/j.1469-8137.2010.03620.x, 2011.

Prentice, I. C., Villegas-Diaz, R., and Harrison, S. P.: Accounting for atmospheric carbon dioxide variations in pollen-based reconstruction of past hydroclimates, Glob. Planet. Change., 211, https://doi.org/10.1016/j.gloplacha.2022.103790, 2022.

Reeves, J. M., Bostock, H. C., Ayliffe, L. K., Barrows, T. T., De Deckker, P., Devriendt, L. S., Dunbar, G. B., Drysdale, R. N., Fitzsimmons, K. E., Gagan, M. K., Griffiths, M. L., Haberle, S. G., Jansen, J. D., Krause, C., Lewis, S., McGregor, H. V., Mooney, S. D., Moss, P., Nanson, G. C., Purcell, A., and van der Kaars, S.: Palaeoenvironmental change in tropical Australasia over the last 30,000 years - a synthesis by the OZ-INTIMATE group, Quaternary Sci. Rev., 74, 97-114, https://doi.org/10.1016/j.quascirev.2012.11.027, 2013a.

Reeves, J. M., Barrows, T. T., Cohen, T. J., Kiem, A. S., Bostock, H. C., Fitzsimmons, K. E., Jansen, J. D., Kemp, J., Krause, C., Petherick, L., and Phipps, S. J.: Climate variability over the last 35,000 years recorded in marine and terrestrial

Deleted: ournal of

Deleted: aphy

Deleted:

archives in the Australian region: an OZ-INTIMATE compilation, Quaternary Sci. Rev., 74, 21-34, https://doi.org/10.1016/j.quascirev.2013.01.001, 2013b.

Renoult, M., Annan, J. D., Hargreaves, J. C., Sagoo, N., Flynn, C., Kapsch, M.-L., Li, Q., Lohmann, G., Mikolajewicz, U., Ohgaito, R., Shi, X., Zhang, Q., and Mauritsen, T.: A Bayesian framework for emergent constraints: case studies of climate sensitivity with PMIP, Clim. Past, 16, 1715–1735, https://doi.org/10.5194/cp-16- 1715-2020, 2020.

Roderick, M. L., Farquhar, G. D., and Greve, P.: On the assessment of aridity with changes in atmospheric CO_2, Water Resour. Res., 51, 5450–5463, https://doi.org/10.1002/2015WR017031, 2015.

Rojas, M.: Sensitivity of Southern Hemisphere circulation to LGM and 4 × CO2 climates, Geophys. Res. Lett., 40, 965-970, https://doi.org/10.1002/grl.50195, 2013.

Rojas, M., Moreno, P., Kageyama, M., Crucifix, M., Hewitt, C., Abe-Ouchi, A., Ohgaito, R., Brady, E. C., and Hope, P.: Southern Westerlies during the last glacial maximum in PMIP2 simulations, Clim. Dynam., 32, 525–548, https://doi.org/10.1007/s00382-008-0421-7, 2009.

Rowe, C., Wurster, C., Zwart, C., Brand, M., Hutley, L., Levchenko, V., and Bird, M.: Vegetation over the last glacial maximum at Girraween Lagoon, monsoonal northern Australia, Quaternary Res., 102, 39-52, https://doi.org/10.1017/qua.2020.50, 2021.

Scheff, J., Seager, R., Liu, H., and Coats, S.: Are Glacials Dry? Consequences for Paleoclimatology and for Greenhouse Warming, J. Climate, 30, 6593-6609, https://doi.org/10.1175/JCLI-D-16-0854.1, 2017.

Schneider von Deimling, T., Held, H., Ganopolski, A., and Rahmstorf, S.: Climate sensitivity estimated from ensemble simulations of glacial climate, Clim. Dynam., 27, 149-163, https://doi.org/10.1007/s00382-006-0126-8, 2006.

Seltzer, A. M., Ng, J., Aeschbach, W., Kipfer, R., Kulongoski, J. T., Severinghaus, J. P., and Stute, M.: Widespread six degrees Celsius cooling on land during the Last Glacial Maximum, Nature, 593, 228–232, https://doi.org/10.1038/s41586-021-03467-6, 2021.

Sidorenko, D., Rackow, T., Jung, T., Semmler, T., Barbi, D., Danilov, S., Dethloff, K., Dorn, W., Fieg, K., Goßling, H. F., Handorf, D., Harig, S., Hiller, W., Juricke, S., Losch, M., Schröter, J., Sein, D. V., and Wang, Q.: Towards multi-resolution

global climate modeling with ECHAM6-FESOM, Part I: model formulation and mean climate, Clim. Dynam., 44, 757–780, https://doi.org/10.1007/s00382-014-2290-6, 2015.

Sime, L. C., Kohfeld, K. E., Le Quéré, C., Wolff, E. W., de Boer, A. M., Graham, R. M., and Bopp, L.: Southern Hemisphere westerly wind changes during the Last Glacial Maximum: model-data comparison, Quaternary Sci. Rev., 64, 104-120, https://doi.org/10.1016/j.quascirev.2012.12.008, 2013.

Sniderman, J. M. K., Hellstrom, J., Woodhead, J. D., Drysdale, R. N., Bajo, P., Archer, M., and Hatcher, L.: Vegetation and climate change in southwestern Australia during the Last Glacial Maximum, Geophys. Res. Lett., 46, 1709–1720, https://doi.org/10.1029/2018GL080832, 2019.

Sueyoshi, T., Ohgaito, R., Yamamoto, A., Chikamoto, M. O., Hajima, T., Okajima, H., Yoshimori, M., Abe, M., O'ishi, R., Saito, F., Watanabe, S., Kawamiya, M., and Abe-Ouchi, A.: Set-up of the PMIP3 paleoclimate experiments conducted using an Earth system model, MIROC-ESM, Geosci. Model Dev., 6, 819–836, https://doi.org/10.5194/gmd-6-819-2013, 2013.

Taylor, K. E., Stouffer, R. J., and Meehl, G. A.: An Overview of CMIP5 and the Experiment Design, Bull. Amer. Meteor., 93, 485–498, https://doi.org/10.1175/BAMS-D-11-00094.1, 2012.

Tierney, J. E., Zhu, J., King, J., Malevich, S. B., Hakim, G. J., and Poulsen, C. J.: Glacial cooling and climate sensitivity revisited, Nature, 584, 569-573, https://doi.org/10.1038/s41586-020-2617-x, 2020a.

Tierney, J. E., Poulsen, C. J., Montanez, I. P., Bhattacharya, T., Feng, R., Ford, H. L., Hönisch, B., Inglis, G. N., Petersen, S. V., Sagoo, N., Tabor, C. R., Thirumalai, K., Zhu, J., Burls, N. J., Foster, G. L., Goddéris, Y., Huber, B. T., Ivany, L. C., Turner, S. K., Lunt, D. J., McElwain, J. C., Mills, B. J. W., Otto-Bliesner, B. L., Ridgwell, A., and Zhang, Y. G.: Past climates inform our future, Science, 370, eaay3701, https://doi.org/10.1126/science.aay3701, 2020b.

Treble, P. C., Baker, A., Ayliffe, L. K., Cohen, T. J., Hellstrom, J. C., Gagan, M. K., Frisia, S., Drysdale, R. N., Griffiths, A. D., and Borsato, A.: Hydroclimate of the Last Glacial Maximum and deglaciation in southern Australia's arid margin interpreted from speleothem records (23–15 ka), Clim. Past, 13, 667-687, https://doi.org/10.5194/cp-13-667-2017, 2017.

Ullman, D. J., LeGrande, A. N., Carlson, A. E., Anslow, F. S., and Licciardi, J. M.: Assessing the impact of Laurentide Ice Sheet topography on glacial climate, Clim. Past, 10, 487–507, https://doi.org/10.5194/cp-10-487-2014, 2014.

Ujvari, G., Wegner, W., Klotzli, U., Horschinegg, M., and Hippler, D.: Sr-Nd-Hf Isotopic Analysis of < 10 mg Dust Samples: Implications for Ice Core Dust Source Fingerprinting, Geochem. Geophys., 19, 60–63, https://doi.org/10.1002/2017GC007136, 2018.

Voldoire, A., Sanchez-Gomez, E., Salas y Mélia, D., Decharme, B., Cassou, C., Sénési, S., Valcke, S., Beau, I., Alias, A. Chevallier, M., Déqué, M., Deshayes, J., Douville, H., Fernan- dez, E., Madec, G., Maisonnave , E., Moine, M.-P., Planton, S., Saint-Martin, D., Szopa, S., Tyteca, S., Alkama, R., Bela- mari, S., Braun, A., Coquart, L., and Chauvin, F.: The CNRM-CM5.1 global climate model: description and basic evaluation, Clim. Dynam., 40, 2091–2121, https://doi.org/10.1007/s00382- 011-1259-y, 2013.

Volodin, E., Mortikov, E., Kostrykin, S., Galin, V., Lykossov, V., Gritsun, A., Diansky, N., Gusev, A., Iakovlev, N., Shestakova, A., and Emelina, S.: Simulation of the modern climate us- ing the INM-CM48 climate model, Russian Journal of Nu- merical Analysis and Mathematical Modelling, 33, 367–374, https://doi.org/10.1515/rnam-2018-0032, 2018.

Wang, T., Wang, N., and Jiang, D.: Last Glacial Maximum ITCZ Changes From PMIP3/4 Simulations, J. Geophys. Res. Atmos., 128, e2022JD038103, https://doi.org/10.1029/2022JD038103, 2023.

Williams, A. N., Ulm, S., Cook, A. R., Langley, M. C., and Collard, M.: Human refugia in Australia during the Last Glacial Maximum and Terminal Pleistocene: a geospatial analysis of the 25–12 ka Australian archaeological record, J. Archaeol. Sci., 40, 4612-4625, https://doi.org/10.1016/j.jas.2013.06.015, 2013.

Wyrwoll, K.-H., and Valdes, P.: Insolation forcing of the Australian monsoon as controls of Pleistocene mega-lake events, Geophys. Res. Lett., 30, 2279, https://doi.org/10.1029/2003GL018486, 2003.

Yan, M., Wang, B., Liu, J., Zhu, A., Ning, L., and Cao, J.: Understanding the Australian Monsoon change during the Last Glacial Maximum with a multi-model ensemble, Clim. Past, 14, 2037–2052, https://doi.org/10.5194/cp-14-2037-2018, 2018.

Yokoyama, Y., Esat, T. M., Thompson, W. G., Thomas, A. L., Webster, J. M., Miyairi, Y., Sawada, C., Aze, T., Matsuzaki, H., Okuno, J., Fallon, S., Braga, J.-C., Humblet, M., Iryu, Y., Potts, D. C., Fujita, K., Suzuki, A., and Kan, H.: Rapid glaciation and a two-step sea level plunge into the Last Glacial Maximum, Nature, 559, 603, https://doi.org/10.1038/s41586-018-0335-4, 2018.

Yukimoto, S., Adachi, Y., Hosaka, M., Sakami, T., Yoshimura, H., Hirabara, M., Tanaka, T., Shindo, E., Tsujino, H., Deushi, M., Mizuta, R., Yabu, S., Obata, A., Nakano, H., Koshiro, T., Ose, T., and Kitoh, A.: MRI-CGCM3 model output

Deleted: ournal of

Deleted: ogical

Deleted: ence

prepared for CMIP5 lgm, served by ESGF, World Data Center for Climate (WDCC) at DKRZ, https://doi.org/10.1594/WDCC/CMIP5.MRMClg, 2015.

Zheng, W., and Yu, Y: Paleoclimate simulations of the mid-Holocene and last glacial maximum by FGOALS, Adv. Atmos. Sci., 30, 684–698, https://doi.org/10.1007/s00376-012-2177-6, 2013.

Zhu, J., Otto-Bliesner, B. L., Brady, E. C., Poulsen, C. J., Tierney, J. E., Lofverstrom, M., and DiNezio, P.: Assessment of equilibrium climate sensitivity of the Community Earth System Model version 2 through simulation of the Last Glacial Maximum, Geophys. Res. Lett., 48, https://doi.org/10.1029/2020GL091220, 2021.

Zhu, J., Otto-Bliesner, B. L., Brady, E. C., Gettelman, A., Bacmeister, J. T., Neale, R. B., Poulsen, C. J., Shaw, J. K., McGraw, Z. S., and Kay, J. E.: LGM Paleoclimate Constraints Inform Cloud Parameterizations and Equilibrium Climate Sensitivity in CESM2, J. Adv. Model. Earth Syst., 14, e2021MS002776. https://doi.org/10.1029/2021MS002776, 2022.